A deep Westerbork survey of areas with multicolor Mayall 4 M plates. II - Optical identifications

Windhorst, R.A.; Kron, R.G.; Koo, D.C.

ASTRONOMY & ASTROPHYSICS
SUPPLEMENT SERIES

Astron. Astrophys. Suppl. Ser. **58,** 39-87 (1984)

A deep Westerbork survey of areas with multicolor Mayall 4 m plates. II. Optical identifications

R. A. Windhorst ([1,+,*]), R. G. Kron ([2,*]) and D. C. Koo ([3,*])

([1]) Sterrewacht Leiden, Postbus 9513, 2300 RA Leiden, The Netherlands
([2]) The University of Chicago, Yerkes Observatory, P.O. Box 0258, Williams Bay, WI 53191, U.S.A.
([3]) Department of Terrestrial Magnetism, Carnegie Institution of Washington, 5241 Broad Branch Road NW, Washington, DC 20015, U.S.A.

Received January 3, accepted April 24, 1984

Summary. — A deep multicolor optical identification program is presented for a complete sample of 302 radio sources that were observed with the Westerbork Synthesis Radio Telescope within 5.52 deg^2 down to $S_{1.4\,\mathrm{GHz}} \gtrsim 0.6$ mJy (5 σ).
Optical identifications are made from multicolor prime focus plates taken with the Kitt Peak 4 meter telescope in the passbands U, J, F and N with approximate respective limiting magnitudes of $\sim$ 23^m.3, 23^m.7, 22^m.7 and 21^m.1.
The astrometry has systematic errors smaller than 0".2-0".3, while the random errors are of order 0".4. The agreement between the radio and optical coordinate frames is on average better than 0".25. Identifications are based on positional coincidence using the likelihood ratio method.
For 171 out of the 302 radio sources likely identifications are proposed with an *a posteriori* identification percentage of 53 %, 14 expected spurious objects (or 5 % of all radio sources), while not more than 4 identifications have been missed. The sample reliability is 92 % and its completeness 98 %.
About 20 % of the identifications are stellar objects, the remaining have extended images or are too faint to be classified. About 15 % of the identifications appear in possible clusters. The identification statistics are roughly constant from field to field, except for the Hercules. 2 field which has an unusually high identification fraction (74 %).
The identification fraction is presented as a function of 21 cm flux density and limiting magnitude, and amounts to 15 % for $1 \lesssim S_{1.4\,\mathrm{GHz}} \lesssim 100$ mJy down to the Palomar Sky Survey limit and 29 % down to the effective 48" Schmidt limit. For $S_{1.4} \lesssim 100$ mJy the identification fraction remains roughly constant with flux density, contrary to the prediction of higher fractions by some models for cosmological evolution.
The magnitude distributions for galaxies plus objects of unknown type generally increase towards fainter magnitudes; the quasar magnitude distributions are also increasing but not as steeply as for the radio galaxies.

Key words : radio sources : general — astrometry — galaxies : radio — cosmology.

1. Introduction.

1.1 BACKGROUND. — During the last decade considerable progress has been made in optical identification programs, carried out with increasingly deeper plate material or CCD-exposures. For instance, the identification history of the bright source 3CR sample is illustrative. While about 65 % of the 3CR could be easily identified on Palomar Sky Survey plates, the remaining 35 % were very difficult to detect optically. Systematic attempts were made by Kristian *et al.* (1974, 1978) on deep 48" Schmidt and Hale 200" plates, by Longair and Gunn (1975) on Hale 200" image tube plates, and by Laing *et al.* (1978) and Gunn *et al.* (1981) using Mayall 4 m plates, Hale 200" plates and CCD images. Only now the identification fraction of the 3CR is approaching 100 % completeness.

Optical identification work on other bright source samples has been extensive. Available data for 4C sources were summarized by Katgert-Merkelijn *et al.* (1980). For the Bologna Survey, identification attempts have been made on deep Palomar 48" plates by Grueff and Vigotti (1975, and references therein), while for a small subsample CCD observations were obtained with the 200" Hale telescope by Allington-Smith *et al.* (1982). Even at their effective limit of $V \lesssim 24^m$ the identification percentage of the Bologna sample does not exceed 80 %, showing that the

(+) Now at : Mount Wilson and Las Campanas Observatories, 813 Santa Barbara Street, Pasadena, CA 91101, U.S.A.

(*) Visiting Astronomer, Kitt Peak National Observatory, operated by the Association of Universities for Research in Astronomy, Inc., under contract with the National Science Foundation.

Send offprint requests to : R. A. Windhorst.

redshift and/or radio luminosity distribution differs already from that at the 3CR level.

At still lower flux densities the identified fraction decreases quickly. The redshift distribution of faint radio sources is probably shifted more towards higher redshifts than that of the bright source surveys, while also an increasing fraction of optically less luminous galaxies is expected due to the correlation between radio power and absolute magnitude below the break of the radio luminosity function (Auriemma *et al.*, 1977).

During the past decade, systematic optical identifications have been attempted for faint radio sources, found in a variety of surveys made with the Westerbok Synthesis Radio Telescope, predominantly at 21 cm. A review of the Westerbork identification programs was given by Katgert-Merkelijn, de Ruiter and Willis (1977). The 1st and 2nd Westerbork Survey (Katgert *et al.*, 1973; and Katgert and Spinrad, 1974, respectively) yielded about 20 % identifications down to the PSS limit. In the 2nd WBK survey the identified fraction was increased to 46 % on deep 098-02 plates made with the Lick 3 m telescope, although with limited statistics. In the 3rd Westerbork Survey (Katgert *et al.*, 1979a) 31 % optical identifications were found on deep Palomar Schmidt plates. The Westerbork Background Survey confirmed the identification percentage on PSS plates (Willis and de Ruiter, 1977) and on deep 48″ IIIaJ Schmidt plates (de Ruiter *et al.*, 1977). The latter authors also found an identified fraction of 47 % on Mayall 4 m IIIaJ plates for a limited subsample.

The identification results of the later Westerbork Surveys were reviewed by Katgert *et al.* (1979b), who noted that radio galaxies appear bluer at fainter magnitudes, which was interpreted as possible color evolution of radio galaxies. One of the purposes of the current survey is to study this suggestion in greater detail, with better statistics, more accurate photometry at fainter magnitude levels, and with spectroscopy.

1.2 Motivation and characteristics of the current survey. — In all surveys fainter than 1 Jy the apparent magnitude distribution shows a strongly increasing number of galaxy identifications at fainter magnitudes. Thus if one could improve upon the magnitude limit, a considerable gain in identification percentage is to be expected. Furthermore, most optical identification programs, especially of the faint radio surveys, have lacked carefully calibrated photometry. Deep optical identification attempts are needed with large optical telescopes and careful photoelectrically-calibrated photometry. This paper is a first attempt to provide such a sample. Rather than obtaining prime focus plates for alteady existing Westerbork areas, we decided to do a new Westerbork Survey of areas with already existing Mayall 4 m prime focus plates, which had been collected during the past years for the purpose of faint galaxy and quasar photometry (Kron, 1978, 1980; Koo, 1981; Koo and Kron, 1982).

The new Westerbork 3 km extension, which became operational in 1980, was used by Windhorst *et al.* (1984, Paper I) to produce high quality synthesis maps of nine selected 4 m fields. The beam size of a 1×12^h observation at 1412 MHz is $12''.5 \times 12''.5$ cosec δ, with position errors of $0''.4$ for the strongest and $\sim 1''.0$ for the faintest point sources. Such small errors allow reliable optical identifications to be made on the 4 m plates using positional coincidence alone. The current survey contains a complete sample of 302 radio sources, defined by a 21 cm peak flux density cut-off at 5 σ (σ = 0.12-0.25 mJy), and by a limiting primary beam attenuation of -7 dB (cut-off radius $r = 0^\circ.464$, which equals the effective 4 m plate radius). Apart from the single field SA57, the nine fields (with a total survey area of 5.52 deg^2) are partially overlapping and thus provide independent checks on radio and optical identification positions, fluxes and photometry.

In section 2 we discuss the astrometry and its reliability. Section 3 decribes the position error distribution, the selection of the optical candidates and the identification method. Section 4 gives the proposed identifications. In section 5 we discuss the identification statistics (also *versus* flux density and limiting magnitude) and present the magnitude distributions.

2. Astrometry.

2.1 Available Mayall 4 m plates. — A collection of good multicolor prime focus plates has been acquired with the Kitt Peak Mayall telescope for several high latitude fields in the selected areas SA57, SA68, SA28 (hereafter referred to as the Lynx area) and an area in Hercules. All areas were chosen for the purpose of faint galaxy photometry. The only selection criterion was the requirement of low galactic absorption.

Multicolor plates were made with the prime focus direct camera, generally using corrector lenses UKB-7 for the IIIaJ emulsions (central plate scale of $18''.59$ mm^{-1}) and BK-7 for the 127-02 and IV-N emulsions (central plate scale $18''.74$ mm^{-1}). Details can be found in Kron (1980) and Koo (1981). Our *UJFN* photometric system is defined by the emulsion+filter combinations : U : IIIaJ+UG5; J : IIIaJ + GG385; F : 127-02 + GG495 and N : IV-N + RG695.

The 127-02 emulsion has a relatively enhanced red response compared to the otherwise similar IIIaF emulsion.

The plates were exposed long enough to be sky limited; i.e. for about 150 min for the U, 45 min for the J, and 60 min for the F and N plates. Limiting magnitudes for stellar objects under good seeing conditions are typically $\sim 24^m.0$ in U and J, $\sim 23^m.0$ in F and $\sim 21^m.5$ in N. Depending on their surface brightness, the effective limits for galaxies can be up to $\sim 1^m.0$ brighter (Koo, 1981).

Table I summarizes the plates that were used for the identification and photometry process. Many more plates are available, but this set represents those of the highest quality. The circular area covered by each plate is about 0.68 deg^2.

2.2 Definition of secondary standard stars on Lick Astrograph plates. — The average star density in astrometric catalogues is not high enough for reliable astrometry on the 4 m plates. Moreover these stars are too bright for easy positional measurement on our plates. Therefore a set of secondary standard stars was selected within each 4 m plate area on astrographic plates, made with the 20″ Lick Carnegie Double Astrograph in 1975. These plates are 8 × 10 inch in size, covering 3.1 × 3.9 degrees at a scale of $55''.06$ mm^{-1}. Typically about 30 AGK-3 stars were

selected as primary standards and their positions were corrected for proper motion to the mean epoch of the Lick Astrograph plates (1975.6). Next we chose for every 4 m plate area 30-40 faint secondary standard stars distributed as regularly as possible.

Positions were measured with the Berkeley PDS 1010A microdensitometer by centring the projected star image on the crosshair by eye. Systematic changes in (X, Y) positions were smaller than 5 μ (0".3) on timescales of a few hours, while the repeatability of individual measurements was 5-10 μ. The Astrograph plate constants were solved by means of a second order polynomial fit, using a routine provided by M. Birkinshaw. Up to five primary standard stars with evidently high residuals — probably due to uncertain proper motion corrections — were omitted from each solution. The overall accuracy of the Astrograph plate solutions was typically 0".4 (7 μ).

2.3 ASTROMETRY ON MAYALL PRIME FOCUS PLATES. — For the 4 m plates we used a similar procedure with the Berkeley PDS, allowing positions to be measured by eye to within 0".1-0".2 (5-10 μ).

A correction for geometrical distortion was applied using Chiu's (1976) distortion coefficients. The geometrical distortion is different for the two corrector lenses, and is a steep function of the radial distance from the geometrical plate centre. It is thus important to use the *actual* coordinates of the optical axis during exposure, which are not always precisely known. In principle one should solve for plate scale and geometrical centre simultaneously. In practice we performed the equivalent by solving for the second order terms.

Good solutions over the 4 m plates were obtained with residuals of order 0".2-0".3 using 25-35 secondary standard stars, after omitting up to five stars with evidently nigh residuals ($\gtrsim$ 2"). Given the 4 m plate solutions, the known (α, δ) coordinates of the radio sources are transformed into their corresponding (X, Y) positions on the *actual* plate, after applying Chiu's inverse distortion corrections.

2.4 OVERALL RELIABILITY OF THE ASTROMETRY. — Effects of plate orientation or of omitting a few secondary standard stars from the fit did not affect the plate solutions at the level of 0".3.

A good check of systematic and random astrometry errors on the 4 m plates is to compare the independent position measurements of objects in the overlapping region of different sets of plates. Figure 1 shows the histogram of position differences. Random errors are of order 0".4 and are a combination of individual measurement errors and some possible proper motion of the secondary standard stars. Systematic position differences are about 0".2-0".3 for the various plate pairs. Their astrometry was based on different sets of secondary standards but again using the *same* primary standards, so systematic differences in the AGK-3 will not show up. Any systematic offsets will also be found empirically in a comparison of the radio and optical position frames and turn out to be small (Sect. 3.5).

3. The identification procedure.

3.1 RADIO AND OPTICAL POSITION ERROR DISTRIBUTIONS. — The precise radio and optical position error distribution is important for a reliable identification procedure based on positional coincidence.

The radio position error distribution was determined empirically in Paper I (Eq. (4)). It is Gaussian in shape and described by signal-to-noise ratio independent coefficients of 0".4-0".5, added in quadrature to terms that are inversely proportional to the peak signal-to-noise ratio. The latter terms are also proportional to the normalized source area R and define a larger error ellipse for extended sources ($R \simeq$ 2-3) than for point sources ($R \simeq 1$). Thus for an extended source a larger area is searched for the optical identification, because it is often not known *a priori* where the correct identification is to be found. The identification of such radio sources could be missed systematically if one omits this scaling with R, as suggested by Perryman (1979a, 1979b).

According to section 2.4 and figure 1 the optical position error distribution can be represented by a Gaussian with dispersion σ = 0".4. The typical intrinsic uncertainty of the AGK-3 positions (~ 0".3) is added in quadrature to the random astrometry error on the 4 m plates. Hence the adopted total optical position error is : $\sigma_\alpha^{\rm opt} = \sigma_\delta^{\rm opt} =$ 0".5. For most optical identifications a position was measured on four plates and the average position was used in the subsequent analysis. Sometimes the dispersion was 0".6 to 0".8, mostly for very low surface brightness galaxies or for objects at the extreme edge of a plate. In such cases this larger dispersion was adopted as the optical position error.

3.2 SELECTION OF CANDIDATE IDENTIFICATIONS. — Given the radio an optical position errors, for every radio optical pair the combined radio optical position errors are defined as :

$$\sigma_\alpha = \sqrt{(\sigma_\alpha^{\rm rad})^2 + (\sigma_\alpha^{\rm opt})^2} \quad \text{and} \quad \sigma_\delta = \sqrt{(\sigma_\delta^{\rm rad})^2 + (\sigma_\delta^{\rm opt})^2} \tag{1}$$

and the normalized radio-optical position difference as :

$$r = \sqrt{\left(\frac{\Delta\alpha}{\sigma_\alpha}\right)^2 + \left(\frac{\Delta\delta}{\sigma_\delta}\right)^2}\,. \tag{2}$$

This defines an error ellipse around each radio source. In this error space we look for the nearest object in r, which due to the ellipticity of the radio beam is not necessarily the closest in position. However, in essentially all cases it is the optical object closest to the radio source.

Most real identifications are found for $r \leqslant 3$ and the total area covered by the combined radio-optical 3 σ error ellipses of all 302 radio sources is 14.9×10^3 arcsec^2. Because the average background density on the 4 m plates amounts to $(12 \pm 2) \times 10^{-4}$ arcsec^{-2}, the expected number of spurious objects with $r \leqslant 3$ is about 18. Indeed for 19 out of 302 sources more than one object appeared within the combined 3 σ error ellipse, generally double galaxies, groups or clusters, for which also the closest object in r was measured. Only in two cases was the magnitude difference between the two candidates much larger than expected for a group or cluster. These are probably chance superpositions of two unrelated objects, discussed in the notes following table IV.

Identification by positional coincidence alone could not always be done for the following classes of objects :

A. Very extended radio sources (doubles with angular sizes $\gtrsim 30''$). — The most likely optical candidate was searched for at an optimally weighted central position, which is not the centre of gravity, but is closer to the actual midpoint (see Paper I and Katgert-Merkelijn *et al.*, 1980).

B. Head-tail and asymmetrical or complex radio sources. — Their most likely optical identification could sometimes be more than 3 σ away from the central radio position, which however can be poorly defined for low surface brightness sources. To some extent the choice of the announced identification may depend on what we expect for this class of radio sources based upon studies of local surveys (for a review see e.g. Miley, 1980).

C. Sources evidently misaligned with the centre of the optical image. — The radio source was more than 3 σ away from the nucleus of a bright spiral galaxy, but located in a spiral arm, sometimes in an optical knot. The radio source is probably related to a star formation region or supernova remnant.

D. Diffuse radio sources with a spectroscopically confirmed candidate. — A few very low surface brightness radio sources could have poorly determined positions or too low formal errors. A spectroscopically confirmed quasar or emission line galaxy was found just outside the 3 σ error box, while it was often displaced along the radio axis, making the identification very probable.

E. Very low surface brightness radio sources without spectroscopy. — A few cases similar to *D*, but without spectroscopic confirmation thus far.

The identification type, morphology and environment were noted by eye from the PDS screen by two independent observers. The agreement between them was generally good and if they did not agree a « ? » is added to the type information listed in table IV. This classification was also done independently for the 16 identifications seen in the overlapping part of two different plates. In the two cases where the classification did not agree, this was understandable in terms of different plate quality. Hence we are confident that the classifications are generally reliable. A more detailed morphology classification is given by Kron *et al.* (1984, Paper III, see also our Fig. 7).

3.3 Average background density and effective 4 m plate limits. — A third important piece of information in the identification procedure is the average background density of objects on the 4 m plates. In each passband we did visual counts of background objects on 1′x1′ PDS scans around every radio source. For most plates these densities are of order 12×10^{-4} arcsec^{-2}, but can amount to up to 30-40 $\times 10^{-4}$ arcsec^{-2} when a group or cluster surrounds the radio source. Furthermore these surface densities varied slightly with passband, galactic latitude, and especially with plate quality. The uncertainty in the background counts around each radio source is rather large due to the small number of objects involved (typically 4-10). Therefore we use in the following analysis for each plate the visually counted background density that was *averaged* over all unidentified radio sources, rather than the poorly determined background density around each individual radio source. Although the latter method would slightly discriminate against radio galaxies in clusters, the difference between the two turns out to be negligible, as shown in section 3.4.

For the *J* and *F* passbands our visual counts were compared with the total counts in SA57 and SA68 done with the automatic methods described by Kron (1978, 1980) and by Koo (1981). The latitude dependence of the star counts has been approximated by using the models of Bahcall and Soneira (1980). The resulting integral star + galaxy counts are given in table II for the various fields, together with our visual counts averaged over the non-identifications, illustrating the effective *J* and *F* plate limits for visual inspection. During the photometry stage of Paper III we noted on each plate the magnitudes of the faintest measured objects. This leads to the slightly more conservative effective plate limits, $U_{\rm lim}$, $J_{\rm lim}$, $F_{\rm lim}$ and $N_{\rm lim}$, also listed in table II. The values of $J_{\rm lim}$ and $F_{\rm lim}$ are consistent with the comparison of our visual background counts with the galaxy + star counts. The value of $J_{\rm lim}$ is also in good agreement with Monte Carlo modelling of the *J* plate limits by Koo (1981), who found that for $\lesssim 23^{\rm m}.8$ his catalogues are more than 95 % complete.

The effective magnitude limits for visual inspection of the 4 m plates are used to give a conservative definition of an optically complete sample : any optical candidate will be part of an *optically complete sample* if it is brighter than the magnitude limits of table II *in at least two passbands.* In addition we include those objects that are at least $0^{\rm m}.75$ brighter than these limits in only one passband. This criterion allows the inclusion of three brighter reliable identifications that were at the edge of a field and could be seen on only one plate.

3.4 The likelihood ratio criterion for optical identifications. — In this section we first assess the reliability of an *individual* identification and then describe how the resulting identification fraction plus the reliability and completeness are obtained for the *total* sample. For this analysis we used the likelihood ratio criterion described by de Ruiter *et al.* (1977), which is comparable to procedures of Richter (1975) and Condon *et al.* (1975). The basic tools which are necessary to understand the results of the current survey are summarized below.

The likelihood ratio method basically assumes that, in the error free case, a radio source and its optical identification coincide in position, and that the true identification is always closer to the radio source than the first contaminating object. The first assumption is not always true for very extended radio sources without a compact core, although the intrinsic radio-optical offsets are known to be small ($\lesssim 0.04$ of the total angular size for 3 CR sources (Macklin, 1981), which would be $< 1''$ in our case). The second assumption is almost always fulfilled because the background density on the 4 m plates is low compared to our very small radio-optical error ellipse.

Given the normalized position difference *r* for a certain radio optical pair, de Ruiter *et al.* define the likelihood ratio (their Eq. (4)) by :

$$LR(r) = \frac{dp(r \mid id)}{dp(r \mid c)} = \frac{r \exp(-r^2/2)\, dr}{2\lambda r \exp(-\lambda r^2)\, dr} = \frac{1}{2\lambda} \exp\left(\frac{r^2(2\lambda - 1)}{2}\right) \quad (3)$$

The likelihood ratio compares the *a priori* probability that, given the object is the correct identification (*id*), it is found between r and $r + dr$, with the probability that a contaminating object (*c*) is found in this ring. The former is given by the Rayleigh distribution, while the latter is a Poisson distribution (in the absence of clustering) and is characterized by $\lambda = \pi\sigma_\alpha\,\sigma_\delta\,\rho_{BG}$, where σ_α and σ_δ are given by equation (1) and the average background density ρ_{BG} is taken from table II. An optical candidate is a likely identification of a given radio source if its likelihood ratio is larger than a certain cut-off value L, which turns out to be about 2. This is a compromise between missing too many real identifications in the tail of the Rayleigh distribution and including too many spurious objects.

For every identification candidate found in the ring between r and $r + dr$, de Ruiter *et al.* define the Bayesian *a posteriori* chance that it is the correct identification, $p(id \mid r)$, and the chance that it is a contaminating object, $p(c \mid r)$. These probabilities depend, albeit not very strongly, on the actual identification fraction, which is defined as :

$$\theta = \frac{N_{id}}{N_{rss}} = \frac{\sum_{\text{all rss}} p(id \mid r)}{N_{rss}}, \qquad (4)$$

where the summation is carried out over all radio sources ($N_{rss} = 302$) in the complete sample. Since θ and $p(id \mid r)$ are not independent we solved for θ iteratively. The sample completeness C is the fraction of all the *real* identifications that actually appear in the sample with $LR \geqslant L$. The sample reliability R is the fraction of the *announced* identification candidates with $LR \geqslant L$ that is expected to be real.

It turns out that most candidates have either $LR \geqslant 5$ or $LR \leqslant 0.1$ and only six have $1.4 \leqslant LR \leqslant 3.0$. Because an error of 50 % in ρ_{BG} will to first order result in an equal error in the LR, the particular value of ρ_{BG} will not influence the identification statistics significantly. Only a few objects would drop from or enter into the sample. For this reason we did not use the poorly determined value of ρ as counted around each individual source.

In principle one could do a likelihood ratio analysis that depends on the magnitude of the candidate found around each radio source. Instead of the average ρ_{BG} down to the plate limit one could take the integral object counts down to the magnitude of the proposed candidate. This would slightly increase the values of LR and thus the number of announced identifications. Our magnitude independent likelihood ratio analysis is more conservative, with perhaps a minor bias against very bright identifications. If the identification with a bright optical candidate was problematic, some criteria other than positional coincidence were used in order to judge their reliability (see Sect. 3.2).

The identification of 25 candidates was not straightforward and additional information was used. For these objects the likelihood ratio method formally does not apply.

3.5 THE RADIO-OPTICAL POSITION DIFFERENCES. — The independently measured radio and optical coordinate systems are compared in table III, where the position differences are averaged over the likely identifications ($LR \geqslant 2$). With a few exceptions most radio-optical offsets are not significant. There are small offsets in both α and δ of SA57 and Hercules.1 due to calibration errors of order $\sim 0''.4 - 0''.5$ in the radio observations. The RA offset in Lynx.1 is due to the self-calibration of the radio map (see Paper I), where the radio reference frame was based on the optical position of the strong radio quasar 55W075. The map of SA68.2 was self-calibrated on the position of the optical identification of 54W057, but here the procedure apparently worked better. In the likelihood ratio analysis the radio-optical position differences were corrected for the average offsets per field.

The observed distribution of the normalized position differences is shown in figure 2a for the sample of 146 identifications with $LR > 2.0$. The Rayleigh distribution is shown for the expected 138.8 identifications with $LR \geqslant 2.0$ and peaks for $r = 1$. The Poisson distribution is drawn for the expected 7.2 contaminating objects. The observed histogram is well represented by the Rayleigh distribution, giving an *a posteriori* justification of the likelihood ratio method. There are 10 objects with $r \geqslant 2$ in excess of the Rayleigh distribution, while about 8 contaminating objects are expected. Although these numbers agree, there might still be a few objects for which r is enhanced due to misalignment of the *intrinsic* radio and optical positions (Macklin, 1981).

Figure 2b shows a vector plot of the absolute radio-optical position differences $\Delta\alpha$ and $\Delta\delta$ for the same sample of 146 identifications, after the average offsets per field (Table III) were applied. The corresponding histograms are not entirely Gaussian in shape because the differences are not normalized with respect to the position errors.

4. The list of optical identifications.

Table IVa gives the identifications in the complete sample of 171 objects discussed in section 5.1. Table IVb gives other identifications that are *not* in the complete radio sample or *not* in the complete optical sample. These are *not* to be used for statistical studies. In figure 3 photographs of the F plates are given as finding charts. In figure 7 also our four-band photographs are given, made from a Grinnell display, as described in Paper III. The contents of tables IVa and IVb are :

Column 1 : source number, consisting of Westerbork Survey number (52 for SA57, 53 for Hercules, 54 for SA68 and 55 for Lynx) and source number. An * denotes an extended or complex source with multiple components. The individual source components are labelled A or B.

Columns 2, 3 : Right Ascension and Declination of the optical identification for the equinox 1950.0.

Column 4 : $\alpha_{rad} - \alpha_{opt} - \langle \alpha_{rad} - \alpha_{opt} \rangle_{field}$

Column 5 : $\delta_{rad} - \delta_{opt} - \langle \delta_{rad} - \delta_{opt} \rangle_{field}$

} with average offsets (in arcsec) from table III.

Column 6 : The normalized position difference r (Eq. (2)).

Column 7 : The likelihood ratio (Eq. (3)).

Column 8 : The identification type given in three categories :

Column 8a : *Object class* (estimated visually from 4 m plate) :

G = galaxy (extended image).
Q = stellar object (not necessarily a quasar).
S = spectroscopically confirmed star.
? = object, but too faint to classify.

Column 8b : *Morphology*. For objects $\gtrsim 4^{m}.0$ above the plate limits we consider :

CD = first ranked galaxy in a cluster or group.
EL = elliptical or lenticular galaxy.
SP = spiral galaxy.
PC = peculiar (explained in the notes below).

For fainter objects we use :

CM = compact, high surface brightness.
FZ = low surface brightness, fuzzy galaxy.

Column 8c : *Environment* :

CL = possible cluster, with $\geqslant 5$ apparently associated galaxies.
GR = group of galaxies, with fewer apparently associated objects.
DB = double galaxy. Another galaxy within one magnitude and one diameter.

Column 9 : *Numbers refer to notes on the optical identification* :

1 = object is stellar, but not blue.
2 = blue object is of (unusually) high surface brightness, or sometimes a red object is of (unusually) low surface brightness.
3 = the identification has a very close companion or an optical jet.
4 = the identification is optically variable.
5 = two or more possible identifications were found in the various radio components of this double or complex radio source. Table IVa lists the identification that we believe to be the correct one from all available data ; table IVb gives the other possible identifications. These cases are discussed individually in the notes.
6 = other notes on the optical object are listed individually below.
7 = detected as X-ray source (Katgert *et al.*, 1983).

Column 9 : *Capitals refer to notes on the radio source morphology*, if relevant for the optical identification. Here the additional 25 objects are classified, for which the likelihood ratio analysis did not give an identification, while still a very likely optical candidate was found. The five corresponding classes are described in section 3.2.

Column 10 : 0 = Reliable identification in the conservative sample of 146 objects.
− 1 = Likely identification in the additional sample of 25 objects. Reason is given in column 9 and in the notes below.
1 = Reliable identification but not in the complete optical sample.
2 = Reliable identification but not in the complete radio sample.

Notes on individual radio source identifications.

Individual notes are given for optical objects that could not be adequately described by columns 8a, 8b, 8c and 9. Notes are also given for the 25 extended or complex radio sources for which the identification was not straightforward. For this latter subsample we classify the suggested identification as solid, very likely, likely or possible. The 21 cm information is taken from Paper I, where contours of extended and complex radio sources are given, in which the positions of the optical objects from the current paper are marked with crosses. The surface brightness (SB) of the radio sources was noted from these contour plots or from a comparison between the contour plots of the high resolution and the low resolution 21 cm maps of Paper I and the 50 cm maps of Windhorst and Oppe (1984; Paper IV). For extended sources the western- and easternmost components are referred to as A and B respectively, while any detectable central component is labelled C. All 50 cm radio information (including spectral index $\alpha = -\log S_{\nu}/\log \nu$) is taken from Paper IV. For a few sources that were asymmetrically resolved at 21 cm a better position was obtained at 50 cm, which in a few doubtful cases clarified the situation. All additional optical information (photometry, spectra) is taken from Paper III, unless stated otherwise.

Name *Notes to table IV.*

52W005 Very red faint galaxy in low surface brightness radio source. Object closer to 50 cm position. Likely identification.

52W013 cD galaxy in Zwicky cluster 1305.4+2941, which is also detected at 2 keV by the Einstein Observatory (Katgert *et al.*, 1983).

52W023 Blue compact emission line galaxy in group. Object just between 21 and 50 cm position, but radio source is of low SB. Very steep spectrum radio source ($\alpha = 1.47$). Solid id.

52W036 Radio source in arm of irregular galaxy with strong emission lines.

52W042 Faint red object in component A of large unequal double source, but no likely id between A and B. Source has no head-tail morphology, hence the red object is unlikely to be the id. Low SB emission connects A and B, so they belong to one (unidentified) source.

53W003 Radio source in arm of interacting pair of spirals. Solid id.

53W027 Faint galaxy close to the head of a triple, V-shaped radio source.

53W034 Faint galaxy in head of a head-tail source with $\alpha = 1.00$. Likely id.

53W039 First ranked cluster galaxy with double nucleus (this is seen on superb *N*-plate only).

53W044 Galaxy with double nucleus (this is seen on superb *N*-plate only).

53W051 Red, possibly stellar, object on radio axis of a resolved, possibly unequal double source, closer to strongest component. Possible id.

53W052 Faint very red emission line galaxy (in group) at the centre of low SB radio source. Very likely id.

53W058 In arm of bright spiral galaxy with double nucleus (or two knots). Closer to the NE knot. Solid id.

53W077 Faint very red galaxy on the radio axis of an unequal double radio source, around the midpoint. Likely id.

53W080 Bright blue quasar with strong emission lines in radio source that is NS extended. Slightly displaced along radio axis. Solid id.

53W086 Faint red galaxy, possibly double, with emission lines in low SB source with flat spectrum ($\alpha = 0.35$). Very likely id.

54W008 Low SB radio source 17″ S of a very bright spiral galaxy. Large error in radio declination of SA68 causes offset. Very likely id.

54W009 Classical double radio source (22″.5), identified with a luminous elliptical galaxy, which is also an X-ray source (Katgert *et al.*, 1983). There is no obvious surrounding cluster, but the object is at the edge of the 4 m plate. The PSS shows a loose group.

54W013 Peculiar compact emission line galaxy (very high SB) with a possible optical jet (or a superimposed object).

54W018 In arm of barred spiral galaxy. Solid id.

54W034 Peculiar disturbed spiral galaxy 8″ N of radio source. Larger error in radio declination could cause offset. Very likely id.

54W049 Faint blue object close to centre of low SB source. Possible id.

54W053 Double galaxy with emission lines 6″ N of low SB radio source. Offset caused by larger error in radio declination. Very likely id.

54W068 Double source with faint blue galaxy (in group) at midpoint. Another faint blue galaxy (also in group) is at position of B, while A is possibly identified with a third galaxy. Both components could be separate radio sources, each identified with a galaxy possibly in the same cluster. Low SB radio emission connects A and B, so they belong to one radio source, with the galaxy of table IVa as the correct id.

55W009 Radio source in arm of a spiral galaxy. Upper limit for radio spectral index $\alpha \leqslant 0.29$, possibly thermal. Solid id.

55W020 Bright spiral galaxy with emission lines. Source close to galaxy nucleus and has steep spectrum ($\alpha = 1.10$) or is variable. Solid id.

55W023 Low SB source, closest to brightest of three galaxies. Possible id.

55W037 4C45.17, classical double with large angular size (114″) at $PA \sim 10°$. Strong emission line elliptical galaxy lies 3″ S of expected position, displaced along radio axis. Undoubtedly the correct id. Blue object coincides with A and may be due to non-thermal (line) emission in the hot spot. A red object is between the 21 and 50 cm position of B.

55W041 Radio source at southern edge of bright elliptical galaxy. Radio source declination probably offset by remaining grating ring in radio map due to vicinity of the very strong source 55W037. Very likely id.

55W043 Bright galaxy in low SB steep spectrum ($\alpha = 0.93$), radio source, whose position may also be affected by the neighbouring 55W037. Likely id.

55W044 Bright galaxy (in group in low SB steep spectrum ($\alpha = 0.90$) source, whose position is probably also affected by 55W037. Likely id.

55W058 Faint red galaxy (in group) in extended, V-shaped source with steep spectrum ($\alpha = 0.92$). Object right at 50 cm position. Very likely id.

55W070 Red stellar object 8″ SW of unequal double radio source but not displaced along axis. Possible id.

55W080 Faint galaxy 6″ E of source that is part of a complex. Vicinity of 55W082 ($\sim$ 30″) presumably affected its position in *RA*. Id possible.

55W082 Faint galaxy displaced 5″ E along axis of strong double radio source with large angular size (53″) at $PA = 94°$. Could be the id, but a high resolution radio map is required for confirmation. For the present, the object is not regarded as the id and is not in table IV.

55W093 Very red galaxy 4″ S of low SB radio source. Possible id.

55W118 Red stellar object, possibly variable, offset from radio position. Close to better 21 cm position of Oort and Windhorst (1984). Likely id.

55W127 Bright G-star. Star is variable at 21 cm (Paper I, and Oort and Windhorst), possibly also at 50 cm ($\alpha = 1.45$!). This is the only *confirmed* galactic identification in the whole survey.

55W136 Faint rich blue cluster, but no obvious identification.

55W137 Complex optical image, possibly two merging spirals.

55W152 Faint red object is closer to radio position. A bright spiral galaxy is probably the id, because it is closer to the 50 cm position.

55W158 Faint galaxy, 5″ NE of G-star (17^m). Although the radio source is variable (Oort and Windhorst, 1984), the galaxy is probably the correct id, since it is closer to the VLA position (Windhorst *et al.*, 1984).

55W161 Triple source with faint red galaxy at component B. In deeper maps (Windhorst *et al.*, 1984) a jet extends from B towards East, so B is the central component and the proposed id is probably correct. The stellar object 12″ N of A is presumably unrelated.

55W163 Stellar object, but red. Variable at 21 cm (Oort and Windhorst, 1984) so it could be a star similar to 55W127.

55W165 Double source with faint red (possibly stellar) object between A and B close to the midpoint. Another faint object is at the position of A, so both components could be unrelated, only A being identified. But low SB radio emission exists between A and B, so both belong to one source, for which the object at the midpoint is given in table IVa.

55W183 Coincides with bright knot on arm of one-armed spiral. Possible supernova remnant or star formation region. Upper limit for spectral index is $\alpha < 0.27$, possibly thermal. Solid id.

55W187 Large classical double (37″) with red galaxy close to midpoint.

55W209 Presumably a head-tail source with as id a double galaxy in the head. Peculiar radio morphology, possibly a curved jet.

55W222 Very red galaxy closer to brightest component of a low SB double radio source. Possible id.

5. Discussion of the results.

5.1 The identification statistics. — The complete sample of table IVa contains 171 proposed identifications, with magnitudes in at least two passbands brighter than the cut-offs of table II, with the exception of three brighter objects at the plate edge (see Sect. 3.3). We refer to the 146 objects with $LR(r) \geqslant 2.0$ as the conservative sample. In this sample we have still missed some very likely identifications. Another 25 objects had formally $LR(r) \leqslant 2.0$, but are believed to be good identifications for reasons mentioned in section 3.2 (see Table IVa and its notes), and are referred to as the additional sample. Only the conservative and the additional sample together form a complete sample.

For the conservative sample figure 4 gives the reliability and completeness as a function of the likelihood ratio cut-off L. Their sum peaks for $L \sim 2.0$. Although this is an arbitrary choice, this likelihood ratio cut-off was adopted in the analysis and in table IVa (Table IVb had a cut-off $L = 1.0$ in order to include a few more objects that are not in a complete sample).

The identification statistics for the whole survey are given at the bottom of table Va for the conservative, the additional, and the total complete sample. The original complete radio sample contains 306 sources, out of which 302 form a complete sample on the 4 m plates. Only 4 sources were outside the exposed part of the 4 m plates (53W049, 53W060, 55W146 and 55W167).

Among the 146 candidates with $LR \geqslant 2$, the expected number of identifications is 142.5 or 47.2 % of all radio sources. For $LR \geqslant 2.0$ there are 138.8 true identifications and 7.2 spurious objects, which can be seen from the cumulative sums in the upper panel of figure 4. The resulting completeness of the conservative sample is 97.4 % (= 138.8/142.5), while its reliability is 95.1 % (= 138.8/146). Thus there are 7.2 spurious objects in this sample, while 3.7 have been missed.

For the additional sample of 25 objects with $LR < 2$ the individual likelihood has been given qualitatively in the notes following table IV. There were 5 proposed solid identifications, 7 were very likely, 6 likely, and 7 possible. We expect that at least 18 out of the 25 objects are indeed good identifications, while at most 7 may turn out to be wrong. Since all available data (including spectra) were used to construct this sample, it will be nearly 100 % complete. Its reliability is about 72 % (= 18/25), while it adds another 6 % (= 18/302) to the identification fraction.

Summarizing, for the total complete sample of 171 objects the *expected* number of identifications is 160.5 (142.5 + 18). Thus for the complete sample of 302 radio sources the total identification fraction is 53.2 %. In total there are 156.8 identifications likely to be *correct*. Thus the overall completeness is 97.7 % (= 156.8/160.5), while its reliability is 91.7 % (= 156.8/171). The total number of spurious objects is expected to be 14.2, while 3.7 real identifications are missing.

As a test of the likelihood ratio method we repeated the identifications in Lynx.3, but rotated the plate 180° on the PDS after the astrometric step. Among 99 radio sources 6 « good identifications » were found, hence the reliability of the procedure is indeed about 93 % as found above.

The identification statistics show that good multicolor 4 m plates yield a considerable improvement in the identified fraction of mJy radio sources over most of the previous deep radio surveys. For example, deep IIIaJ Schmidt plates yield identification percentages of ~ 30 % with J limits of $22^{m}.0$-$22^{m}.5$. De Ruiter *et al.* (1977) found that IIIaJ 4 m plates increased their identification percentage to 47 %, based on 14 new identifications that were not seen on their IIIaJ 48″ plates. They mentioned an effective 4 m plate limit of ~ $23^{m}.5$, while we found $J_{lim} \sim 23^{m}.7$. The 6 % difference in identification percentage is presumably due to the use of multicolor plates in our case. In particular, Paper III shows that some fraction (~ 8 %) of all identifications are faint very red galaxies that *only* show up on the F and N plates. This is also reflected by the larger number of upper limits in the U and J magnitude distributions of section 5.4.

5.2 Variations between fields. — The identification statistics for each of the LBDS fields are listed in table Va, together with the average for each of the four areas. Table Vb shows the identification content for the nine LBDS fields. The average of the identification percentage over the nine fields is 52.8 ± 8.6 %, where the dispersion is determined from the field-to-field variations. The identification percentage of the four Lynx fields, the two SA68 fields and Hercules.1 are fully consistent with the survey average. The percentage in SA57 (43 %) is not significantly below the survey average. However, the very high identified fraction in the Hercules.2 field (74 %) differs from the survey average at the 2.5 σ level. This

very high identification percentage is not due to higher plate quality, because the Hercules.2 plates were of average depth, apart from the exceptionally good N-plate (but this plate confirmed only two candidates that would have been rejected without it). Although for a survey of 9 fields with an average identification percentage of 53 % the occurence of one field with 74 % identifications is only significant at the 90 % level, we want to mention in this context a few other pecularities of the Hercules.2 field.

During the radio reduction it was noted that Hercules.2 contained a 2 σ excess in its number of sources with respect to the expectation for its noise and effective area. It also contained a 2 σ excess in its number of resolved or extended sources, especially several complex, low surface brightness sources, of the type often found amongst low radio power ellipticals in clusters. Amongst the 28 announced identifications in Hercules.2, seven are indeed in a cluster or group. Table Vb shows that this is not unreasonably large since the other fields have on average about 4 to 5 clusters or groups. On the other hand, there are 8 quasars in Hercules.2, while the total number of quasars in the whole survey is 35. The other fields have on average about 2 to 3 quasars per field, with the exception of the Lynx.2 field, which has 9 quasars. Again the numbers of quasars in Hercules.2 and Lynx.2 are not unreasonably large, although at the boundary of being significant. However, most of *both* the clusters and quasars in Hercules.2 occur in a small area of about 0.1 deg^2, while the total area covered by the Hercules.2 field is about 0.6 deg^2. In Lynx.2 two groups of four quasars occur in two even smaller areas (each of 0.05 – 0.1 deg^2), in this case without any neighbouring radio selected clusters or groups.

In conclusion, the identification statistics are in general not indicative of anisotropies on scales of degrees. Apparent peculiarities, like the quasars and clusters in the Hercules.2, field and the quasars in Lynx.2, should be studied with larger samples and spectroscopic redshifts.

5.3 IDENTIFICATION FRACTION *versus* 1.4 GHz FLUX DENSITY AND LIMITING MAGNITUDE. — The identification fraction as a function of flux density and limiting magnitude reflects the combined effects of the radio source redshift distribution and their absolute magnitude distribution. That is, the integral over redshift of the epoch dependent bivariate (radio-optical) luminosity function will yield this distribution.

The observed bivariate flux density distribution, or its semi-integral form, $ID\ \%\ (S_{1.4}, m < m_{\rm lim})$, already yields some constraints on models for cosmological evolution. Swarup *et al.* (1982) presented low frequency identification statistics in the form $ID\ \%(S_{408}, m < m_{\rm PSS})$, i.e. the fraction of radio sources that is identified as a function of 408 MHz flux in an optical identification program down to the limit of the Palomar Sky Survey ($J \simeq B \lesssim 21\overset{\rm m}{.}0$, $F \simeq r \lesssim 20\overset{\rm m}{.}0$). This percentage decreases quickly from $\sim 65\ \%$ at the 3 CR level ($S_{1.4} \gtrsim 3.5$ Jy) to $\sim 15\ \%$ at the Bologna level ($S_{1.4} \gtrsim 300$ mJy) and to $\sim 10\ \%$ at 10 mJy. With these data Swarup *et al.* could reject or refine some of the existing models for cosmological evolution, which predicted too many identifications down to the PSS limit at low flux densities.

Table VI and figure 5 give the $ID\ \%\ (S_{1.4}, m < m_{\rm lim})$ of the current survey down to various magnitude limits. The two points at 0.39 and 1.11 mJy are derived from the VLA survey in Lynx.2 (Windhorst *et al.*, 1984).

The likelihood ratio analysis has been done for the following effective plate limits, requiring objects to be brighter than these limits in at least two passbands :

1) *The* 4$^{\rm m}$ *plate limit* :

$$U \leqslant 23\overset{\rm m}{.}3,\quad J \leqslant 23\overset{\rm m}{.}7,\quad F \leqslant 22\overset{\rm m}{.}7,\quad N \leqslant 21\overset{\rm m}{.}1.$$

2) *The* 48″ *Schmidt limit* :

$$U \leqslant 21\overset{\rm m}{.}75,\quad J \leqslant 22\overset{\rm m}{.}25,\quad F \leqslant 21\overset{\rm m}{.}25,\quad N \leqslant 19\overset{\rm m}{.}5.$$

3) *The PSS limit* :

$$U \leqslant 20\overset{\rm m}{.}0,\quad J \leqslant 21\overset{\rm m}{.}0,\quad F \leqslant 20\overset{\rm m}{.}0,\quad N \leqslant 18\overset{\rm m}{.}5.$$

The last is roughly equivalent to requiring that $B \lesssim 21\overset{\rm m}{.}0$ and $r \lesssim 20\overset{\rm m}{.}0$. The statistical error in the $ID\ \%$ is $\sigma_{ID\%} = \sqrt{(ID\ \% \times (100 - ID\ \%)/n)}\ \%$, where n is the number of radio sources per bin, and is only drawn in figure 5 for the 4 m plate limits in order not to overcrowd the figure.

Figure 5 shows that the identification percentage down to the 4 m plate limit increases slowly from about 45 % around 1 mJy to about 60 % around 10 mJy, while it reaches 70-100 % for $S_{1.4} \geqslant 100$ mJy. The latter is consistent with the 80 % identified fraction of Allington-Smith *et al.* (1982) at $S_{1.4} \sim 500$ mJy down to $m_r \simeq 23\overset{\rm m}{.}0$. The identification percentage down to the effective 48″ limit, is essentially constant (29 %) for $1 \leqslant S_{1.4} \leqslant 100$ mJy, but brighter than that, the $ID\ \%\ (S_{1.4}, m \leqslant m_{48''})$ increases to $\sim 50\ \%$.

The identification percentage down to the effective PSS limit remains largely constant at $\sim 15\ \%$ from 100 mJy even down to 1 mJy. This is consistent with the data of de Ruiter *et al.* (1977), whose $ID\ \%\ (S_{1.4}, m < m_{\rm PSS})$ is plotted as open triangles in figure 5. For $S_{1.4} > 200$ mJy the percentage might increase somewhat, although our statistics are limited. Our data are compared with the predictions of model 4b of Wall *et al.* (1980) and Robertson's (1980) free form model of the spatial distribution of radio galaxies and quasars, after transforming the 408 MHz flux scale to 1412 MHz using $\langle \alpha \rangle = 0.75$. The fact that the $ID\ \%\ (S_{1.4}, m < m_{\rm PSS})$ remains about 15 % down to ~ 0.4 mJy is not in concordance with the WPL models because these predict fractions that exceed 30 % for $S_{1.4} \leqslant 10$ mJy. This is because these models were based solely on redshift distributions for $S_{1.4} \gtrsim 3$ Jy. A model that is consistent with the data is Robertson's free-form model although it might not be optimal for $S_{1.4} \sim 100$ mJy. His evolution function at high radio powers is similar to the direct estimates of the epoch dependent radio luminosity function made from bivariate flux density distributions (for a review see van der Laan and Windhorst, 1982).

The results discussed above demonstrate that the actual redshift and absolute magnitude distribution of faint radio sources could be quite different from that assumed in several models. The rather low identification percentage at low flux densities ($S_{1.4} < 100$ mJy, but especially

$S_{1.4} \leqslant 10$ mJy), may be explained by a distribution towards higher redshift or fainter absolute magnitudes or both.

5.4 THE U, J, F AND N MAGNITUDE DISTRIBUTIONS. — The apparent magnitude distribution is of cosmological importance because it reflects the radio source redshift distribution in combination with the absolute magnitude distribution. In this section we present the magnitude distribution in the passbands U, J, F and N for the complete sample of 170 extragalactic identifications, which consists of 35 stellar objects (Q + Q ?), 121 extended objects (G + G ?) and 14 objects of unknown type (?). Figures 6a, 6b, 6c and 6d give the magnitude distributions $A(U)$, $A(J)$, $A(F)$ and $A(N)$ respectively. Because U plates lacked in Lynx.1 and Lynx.4, there are fewer objects in figure 6a. Stellar objects are plotted separately, while the objects of unknown type are combined with the distribution of the extended objects. The number of extended objects in the faintest magnitude bins is at least three times larger than the number of stellar objects, moreover because the latter is likely to be overestimated since the number of galaxies misclassified as quasars will probably be larger than the number of quasars that are misclassified as galaxies. Since the faint extended objects outnumber the faint stellar objects we expect that the unclassified objects will turn out to be predominantly galaxies.

The vertical dashed lines in figure 6 denote the average plate limits (Table III). If objects are invisible or too faint to be photometered in one or two passbands, they were represented in figure 6 by a magnitude upper limit at the position of the corresponding plate limit. Our definition of a complete sample (objects visible in at least two passbands) has only minor implications for the distributions. Namely, if we relax the conservative definition of a complete sample by including all objects that could be photometered in at least one passband, only 11 additional objects are found, raising the identification percentage from 53.2 % to 56.6 %. This would only slightly enhance the histograms, as shown by the dashed lines in figure 6.

Galaxies.

The U and J magnitude distributions of galaxies increase rather steeply with fainter magnitude essentially down to the plate limits. This effect would only be enhanced if some fraction of the announced quasars with $U, J \geqslant 22^{m}.5$ were in fact galaxies. Furthermore, even after all upper limits in U and J are discarded, the $A(U)$ and $A(J)$ still show a strongly increasing number of galaxies down to $U \sim 23^{m}.0$ and $J \sim 23^{m}.5$. Our $A(J)$ for galaxies is consistent with that of Willis and de Ruiter (1977), who found a strongly increasing number of galaxy identifications for $21^{m} \leqslant J \leqslant 22^{m}$ among radio sources with fluxes in the range $10 \leqslant S_{1.4} \leqslant 1000$ mJy.

On the other hand the F and N magnitude distributions for galaxies increase more slowly towards fainter magnitudes and seem to flatten for $F \geqslant 21^{m}$, while in N it apparently reaches a maximum for $N \sim 19^{m}.5$. Because the N-emulsions have the largest differences in quality, the N-plate limit may have been over- or underestimated for several fields. This could explain part of the apparent lack of objects about one magnitude above the claimed average N-plate limit and the relatively larger number of objects beyond $N \gtrsim 21^{m}$.

Our $A(F)$ for galaxies is consistent with that of Perryman *et al.* (1982), who found that most of their 12 radio galaxy identifications ($S_{1.4} \gtrsim 15$ mJy) were in the range $19^{m} \lesssim m_{r} \lesssim 22^{m}$. It is also similar to that of Allington-Smith *et al.* (1982), who found most of their 33 galaxies with $S_{1.4} \sim 500$ mJy in the range $19^{m} \lesssim m_{r} \lesssim 23^{m}$, and that of Grueff and Vigotti (1977), who found a strong increase of galaxies with $S_{1.4} \gtrsim 300$ mJy for $19^{m}.5 \lesssim r \lesssim 20^{m}.5$. The latter two samples may not be completely comparable to ours due to the large difference in covered radio flux.

Extrapolating the magnitude distributions in figure 6 it is expected that the unidentified 47 % of the radio sources will extend to several magnitudes below the 4 m plate limits. However, since the magnitude distributions generally increase towards fainter magnitudes, most unidentified radio sources could in fact show up within two or three magnitudes below the 4 m plate limits. A precise measurement of the radio galaxy magnitude distribution below the 4 m plate limits would be a strong boundary condition on models for cosmological evolution, especially regarding a possible redshift cut-off. This is an important challenge to high throughput CCD-detectors on large optical reflectors.

Quasars.

The quasar magnitude distributions increase more gradually towards fainter magnitudes than for galaxies. Of course, misclassified galaxies may confuse the picture for quasars one or two magnitudes above the plate limits. The quasar magnitude distribution of Grueff and Vigotti (1977) peaks for $r \sim 17^{m}.5$ in a sample with $S_{1.4} \gtrsim 3$ Jy, and for $F \sim r \sim 19^{m}.5$ in a sample with $S_{1.4} \geqslant 300$ mJy, while that of Allington-Smith *et al.* (1982) also peaks for $r \sim 20^{m}$ in a sample with $S_{1.4} \gtrsim 300$ mJy. The quasar magnitude distribution of Willis and de Ruiter (1977) peaks for $19^{m} \lesssim J \lesssim 21^{m}$ in a sample with $S_{1.4} \gtrsim 10$ mJy.

If the apparent dependence of the quasar magnitude distribution on radio flux is not due to galaxy contamination (in our case) or to the eye estimated magnitudes of Willis and de Ruiter or Grueff and Vigotti, it presumably reflects the bivariate luminosity function of quasars, since our quasars are *also* 10 to 1000 times fainter in the radio than those of Willis and de Ruiter and of Grueff and Vigotti.

Acknowledgements.

We thank the Kitt Peak National Observatory for the allocation of telescope time and for providing financial assistance for travel on several occasions. We also thank Bill Schoening for his many years of help in the photographic work.

This work was partially supported by NSF grants 79 20994 and NSF 81 21653 of the United States and by NATO grant 1479. RAW acknowledges the Netherlands Organization for the Advancement of Pure Research (ZWO) for the ASTRON/ZWO grant 19-23-009 during the course of this research, as well as for several travel grants.

We are grateful to Mark Birkinshaw, Donald Hamilton and Peter Katgert for their astrometry programs. RAW acknowledges the Berkeley Astronomy Department for hospitality during several working visits. RGK and DCK acknowledge the hospitality of the Sterrewacht in Leiden. DCK began this work at Berkeley and thanks Dr. I. King for financial support.

We thank Peter Katgert and Rien de Grijp for helpful discussions and Peter Katgert and Harry van der Laan for a critical reading of the manuscript and their continuous interest for the project. We thank Wanda van Grieken, Liesbeth van der Poel and Petra Steehouwer for a careful typing of the manuscript, Sjaak Ober for drawing the figures and Wim Brokaar and Richard Dreiser for making the photographs. Geoffrey van Heerde and Marc Oort are acknowledged for their help in the final stage of the wordprocessing.

References

Auriemma, C., Perola, G. C., Ekers, R., Fanti, R., Lari, C., Jaffe, W., Ulrich, M. H. : 1977, *Astron. Astrophys.* **57,** 41.
Allington-Smith, J. R., Perryman, M. A. C., Longair, M. S., Gunn, J. E., Westphal, J. A. : 1982, *Mon. Not. R. Astron. Soc.* **201,** 331.
Bahcall, J. N., Soneira, R. M. : 1980, *Astrophys. J. Suppl. Ser.* **44,** 73.
Chiu, L.-T. G. : 1976, *Publ. Astron. Soc. Pac.* **88,** 803.
Condon, J. J., Balonek, T. J., Jauncey, D. L. : 1975, *Astron. J.* **80,** 887.
Grueff, G. V., Vigotti, M. : 1975, *Astron. Astrophys. Suppl. Ser.* **20,** 57.
Grueff, G. V., Vigotti, M. : 1977, *Astron. Astrophys.* **54,** 475.
Gunn, J. E., Hoessel, J. G., Westphal, J. A., Perryman, M. A. C., Longair, M. S. : 1981, *Mon. Not. R. Astron. Soc.* **194,** 111.
Katgert, P., Katgert-Merkelijn, J. K., le Poole, R. S., van der Laan, H. : 1973, *Astron. Astrophys.* **23,** 171.
Katgert, J. K., Spinrad, H. : 1974, *Astron. Astrophys.* **35,** 393.
Katgert-Merkelijn, J. K., de Ruiter, H. R., Willis, A. G. : 1977, in *Radio Astronomy and Cosmology*, IAU Symp. No. **74,** D. L. Jauncey, ed. (Reidel, Dordrecht) p. 165.
Katgert, P., de Bruyn, A. G., Willis, A. G. : 1979a, *Astron. Astrophys. Suppl. Ser.* **36,** 213.
Katgert, P., de Ruiter, H. R., van der Laan, H. : 1979b, *Nature* **280,** 20.
Katgert-Merkelijn, J., Lari, C., Padrielli, L. : 1980, *Astron. Astrophys. Suppl. Ser.* **40,** 91.
Katgert, P., Thuan, T. X., Windhorst, R. A. : 1983, *Astrophys. J.* **275,** 1.
Koo, D.C. : 1981, Ph. D. Thesis, University of California, Berkeley.
Koo, D. C., Kron, R. G. : 1982, *Astron. Astrophys.* **105,** 107.
Kristian, J., Sandage, A., Katem, B. : 1974, *Astrophys. J.* **191,** 43.
Kristian, J., Sandage, A., Katem, B. : 1978, *Astrophys. J.* **219,** 803.
Kron, R. G. : 1978, Ph. D. Thesis, University of California, Berkeley.
Kron, R. G. : 1980, *Astrophys. J. Suppl. Ser.* **43,** 305.
Kron, R. G., Koo, D. C., Windhorst, R. A. : 1983, *Astron. Astrophys.*, submitted (Paper III).
van der Laan, H., Windhorst, R. A. : 1982, in *Astrophysical Cosmology* Proceedings of the Vatican Study Week on Cosmology and Fundamental Physics, H. A. Brück, G. V. Coyne, M. S. Longair, eds. (Pontificiae Academiae Scientiarum, Vaticano) p. 349.
Laing, R. A., Longair, M. S., Riley, J. M., Kibblewhite, E. J., Gunn, J. E. : 1978, *Mon. Not. R. Astron. Soc.* **183,** 547.
Longair, M. S., Gunn, J. E. : 1975, *Mon. Not. R. Astron. Soc.* **170,** 121.
Macklin, J. T. : 1981, *Mon. Not. R. Astron. Soc.* **196,** 967.
Miley, G. K. : 1980, *Ann. Rev. Astron. Astrophys.* **18,** 165.
Oort, M. J. A., Windhorst, R. A. : 1984, *Astron. Astrophys.*, submitted.
Perryman, M. A. C. : 1979a, *Mon. Not. R. Astron. Soc.* **187,** 223.
Perryman, M. A. C. : 1979b, *Mon. Not. R. Astron. Soc.* **187,** 683.
Perryman, M. A. C., Longair, M. S., Allington-Smith, J. R., Fielden, J. : 1982, *Mon. Not. R. Astron. Soc.* **201,** 957.
Richter, G. A. : 1975, *Astron. Nachr.* **296,** 65.
Robertson, J. G. : 1980, *Mon. Not. R. Astron. Soc.* **190,** 143.
de Ruiter, H. R., Willis, A. G., Arp, H. C. : 1977, *Astron. Astrophys. Suppl. Ser.* **28,** 211.
Swarup, G., Subrahmanya, C. R., Venkatakrishna, K. L. : 1982, *Astron. Astrophys.* **107,** 190.
Wall, J. V., Pearson, T. J., Longair, M. S. : 1980, *Mon. Not. R. Astron. Soc.* **193,** 683.
Willis, A. G., de Ruiter, H. R. : 1977, *Astron. Astrophys. Suppl. Ser.* **29,** 103.
Windhorst, R. A., van Heerde, G. M., Katgert, P. : 1984, *Astron. Astrophys. Suppl. Ser.*, this volume (Paper I).
Windhorst, R. A., Miley, G. K., Owen, F. N., Kron, R. G., Koo, D. C. : 1984, *Astrophys. J.*, in press (Paper V).
Windhorst, R. A., Oppe, J. : 1984, *Astron. Astrophys. Suppl. Ser.*, submitted (Paper IV).

1984A&AS...58...39W

TABLE I. — *List of Mayall prime focus plates used.*

Field	α_{1950} H M S	δ_{1950} o ' "	MPF	Emuls.	Filter	t_{exp} (min)	HA (end)	Airmass (mid)	Seeing (σ/")	Comments/ Observer(*)
SA57	13 06 15	29 39 08	3314	IIIaJ	UG-5	135	1W19	1.01	0.86	
	13 06 15	29 39 04	1053	IIIaJ	GG385	45	0W33	1.01	0.68	D.Wells
	13 06 16	29 38 56	1562	IIIaJ	GG385	45	0E16	1.01	0.70	
	13 06 16	29 38 56	3622	IIIaJ	GG385	55	0W42	1.00	0.67	
	13 06 15	29 39 04	1572	127-02	GG495	60	1W51	1.05	0.63	
	13 06 15	29 39 08	3315	IV-N	RG695	60	2W54	1.15	0.74	UBK-7
Her.1	17 18 56	49 58 08	3324	IIIaJ	UG-5	145	1W45	1.06	0.79	
	17 18 56	49 58 08	1138	IIIaJ	GG385	60	2W57	1.19	0.76	
	17 19 07	49 59 10	1129	127-02	GG495	75	2W09	1.10	0.75	
	17 19 08	49 59 10	1574	127-02	GG495	60	0E05	1.06	0.64	
	17 18 56	49 59 08	3159	IV-N	RG695	50	1W12	1.06	0.55	
Her.2	17 14 53	50 12 36	3727	IIIaJ	UG-5	115	4W35	1.38	0.83	R.Windhorst
	17 14 53	50 12 36	3725	IIIaJ	GG385	45	1W38	1.09	0.81	H.Butcher
	17 14 53	50 12 36	3726	IIIaJ	GG385	35	4W36	1.56	0.90	H.Butcher
	17 14 56	50 12 33	1573	127-02	GG495	60	1E08	1.11	0.65	
	17 14 52	50 12 43	3160	IV-N	RG695	60	2W23	1.13	0.52	
SA68.1	00 14 53	15 36 40	3164	IIIaJ	UG-5	120	2W12	1.09	0.59	
	00 14 53	15 36 37	1286	IIIaJ	GG385	45	2W37	1.22	0.56	
	00 14 53	15 36 28	1283	127-02	GG495	60	1E10	1.13	0.63	I.King
	00 14 53	15 36 28	1284	127-02	GG495	60	0E04	1.05	0.65	I.King
	00 14 53	15 36 34	3156	IV-N	RG695	60	1E44	1.21	0.56	
SA68.2	00 14 41	16 81 51	3442	IIIaJ	UG-5	150	1W30	1.04	0.81	Racine Prisms
	00 14 41	16 19 12	1295	IIIaJ	GG385	45	1W44	1.10	0.52	
	00 14 45	16 18 31	1293	127-02	GG495	60	0E22	1.06	0.65	I.King
	00 14 41	16 18 52	3161	IV-N	RG695	60	3E16	1.67	0.62	
Lynx.1	08 38 02	44 58 38	1290	IIIaJ	GG385	41	2E05	1.17	0.81	No U-plate
	08 38 02	44 58 38	1403	127-02	GG495	60	1E28	1.12	0.78	PSF not round
	08 38 02	44 58 38	3620	IV-N	RG695	60	2W44	1.14	0.74	
	08 38 02	44 58 38	3621	IV-N	RG695	60	3W54	1.33	0.77	
Lynx.2	08 41 48	44 47 52	3619	IIIaJ	UG-5	150	1W26	1.03	0.57	
	08 41 48	44 47 52	1288	IIIaJ	GG385	45	3E51	1.56	0.71	
	08 41 48	44 47 52	1289	IIIaJ	GG385	45	3E04	1.34	0.69	
	08 41 48	44 47 52	1298	127-02	GG495	65	3E14	1.42	0.56	I.King
	08 41 48	44 47 52	1299	127-02	GG495	65	2E04	1.19	0.49	I.King
	08 41 48	44 47 52	3626	IV-N	RG695	45	2E53	1.30	1.17	
	08 41 48	44 47 52	3627	IV-N	RG695	60	1W47	1.15	1.12	
Lynx.3	08 45 30	44 35 30	3630	IIIaJ	UG-5	140	2W30	1.06	1.06	
	08 45 30	44 35 30	1409	IIIaJ	GG385	45	2E41	1.26	0.75	Gold spots
	08 45 30	44 35 30	1411	127-02	GG495	60	0E05	1.03	0.53	I.King
	08 45 30	44 35 30	3631	IV-N	RG695	60	3W32	1.26	0.68	
	08 45 30	44 35 30	3632	IV-N	RG695	50	4W37	1.55	0.73	
Lynx.4	08 34 29	45 09 44	1576	IIIaJ	GG385	45	0W45	1.03	0.81	No U-plate
	08 34 29	45 09 44	1412	127-02	GG495	60	1W24	1.04	0.65	I.King
	08 34 29	45 09 44	1413	127-02	GG495	60	2W31	1.12	0.70	I.King
	08 34 29	45 09 44	3618	IV-N	RG695	60	1E22	1.10	0.59	
	08 34 29	45 09 44	3617	IV-N	RG695	60	2E29	1.25	0.64	

(*) Observers are R.Kron or D.Koo unless stated otherwise.

TABLE III. — *Radio-optical position offsets for the identifications with LR > 2.*

Field	$\langle\alpha_r - \alpha_o\rangle$	±m.e.	$\langle\delta_r - \delta_o\rangle$	±m.e.	N_{id}(LR>2)
SA57	+0".54	±0".28	+0".49	±0".29	12
Her.1	+0.43	±0.20	-0.47	±0.26	13
Her.2	+0.05	±0.19	+0.02	±0.26	27
SA68.1	+0.24	±0.30	+0.12	±0.83	13
SA68.2	-0.21	±0.28	-0.41	±0.50	13
Lynx.1	+0.69	±0.23	+0.06	±0.23	13
Lynx.2	-0.27	±0.25	-0.06	±0.29	23
Lynx.3	+0.20	±0.30	-0.27	±0.23	18
Lynx.4	+0.03	±0.19	+0.06	±0.20	14
Weighted average over whole survey	+0".16	±0".09	-0".07	±0".12	146
After correction offsets per field	+0.03	±0.09	-0.01	±0.12	146

1984A&AS...58...39W

TABLE II. — *Average background densities and effective plate limits.*

Field	b^{II}	N(J<23.5)	N(J<23.75)	N(J<24.0)	N_{obs}(J<J_{lim})	U_{lim}	J_{lim}
		(all in 10^{-4} arcsec^{-2})					
	°					m	m
SA57	+85	8.4	10.8	13.6	11.8 ±3.3	23.75	23.75
Her.1	+35	11.2	13.8	16.7	14.9 ±2.5	23.0	23.5
Her.2	+35	11.2	13.8	16.7	15.9 ±1.7	23.25	23.5
SA68.1	-46	8.9	11.3	14.1	12.0 ±1.4	23.0	23.75
SA68.2	-46	8.9	11.3	14.1	12.0 ±2.0	23.5	23.75
Lynx.1	+38	8.9	11.3	14.1	10.8 ±2.0	-	23.75
Lynx.2	+38	8.9	11.3	14.1	13.2 ±0.5	23.5	23.75
Lynx.3	+39	8.9	11.3	14.1	12.3 ±3.1	23.25	23.75
Lynx.4	+37	8.9	11.3	14.1	10.9 ±1.3	-	23.5
					Average ± s.d.	23.3 ±0.3	23.7 $\pm^{0.1}$

Field	b^{II}	N(F<22.5)	N(F<22.75)	N(F<23.0)	N_{obs}(F<F_{lim})	F_{lim}	N_{lim}
		(all in 10^{-4} arcsec^{-2})					
	°					m	m
SA57	+85	8.6	10.0	11.6	11.4 ±1.8	23.0	21.0
Her.1	+35	13.1	14.7	16.7	15.8 ±1.6	22.25	20.75
Her.2	+35	13.1	14.7	16.7	17.3 ±3.4	22.75	21.75
SA68.1	-46	9.4	10.8	12.5	11.8 ±0.9	22.5	21.25
SA68.2	-46	9.4	10.8	12.5	11.9 ±2.5	22.75	21.0
Lynx.1	+38	9.6	11.0	12.7	11.1 ±1.2	22.75	20.75
Lynx.2	+38	9.6	11.0	12.7	12.9 ±1.2	22.75	21.25
Lynx.3	+39	9.6	11.0	12.7	12.0 ±1.7	22.75	21.0
Lynx.4	+37	9.6	11.0	12.7	11.3 ±2.3	23.0	20.75
					Average ± s.d.	22.7 ±0.2	21.1 $\pm^{0.3}$

Col. 1 Field name
Col. 2 Galactic latitude
Col.3,4,5 Integral model star counts (Bahcall and Soneira 1980) plus observed galaxy counts (Kron 1980, Koo 1981) in units of arcsec^{-2}, down to specified J and F magnitude limits.
Col. 6 Visual object counts on 1'x1' PDS scans, averaged over about 20 non-identifications per plate (in arsec^{-2}).
Col. 7,8 Estimated plate limits.

TABLE IVa. — *The list of optical identifications in the complete sample.*

NAME	RA(1950) H M S	DEC(1950) D M S	DRA (")	DDEC (")	R	LR	ID	MORPH	ENVIR	NOTES	CODE
52W005	13 4 27.44	29 31 17.4	-4.5	0.1	3.70	0.09	G			E	-1
52W008	13 5 0.65	29 18 26.6	-0.6	0.6	1.12	117.87	G		CL		0
52W012	13 5 23.81	29 19 2.9	-0.5	-1.5	1.87	38.80	G		CL		0
52W013	13 5 26.31	29 41 46.9	-0.8	-0.5	0.96	88.10	G	CD	CL	6	0
52W017	13 5 42.03	29 35 42.2	-0.3	-0.7	0.83	130.04	?				0
52W020	13 5 57.51	30 0 1.8	0.0	0.9	0.70	101.39	G	SP			0
52W022	13 6 10.56	29 50 19.6	1.1	0.9	1.87	51.34	?				0
52W023	13 6 11.55	29 42 26.3	-1.5	7.4	5.22	0.00	G	CM	GR	D	-1
52W034	13 6 45.50	29 30 3.8	1.8	-1.1	1.48	18.91	G		GR		0
52W037	13 6 53.39	29 38 0.7	-0.8	-0.2	0.82	119.11	G	SP		2	0
52W038	13 6 55.72	29 22 46.6	1.2	0.6	1.42	51.41	G			4	0
52W039	13 7 1.15	30 2 3.9	1.9	2.6	2.38	5.59	?				0
52W044	13 7 14.57	29 41 26.2	-1.5	-0.5	1.42	31.57	G	CM			0
52W047	13 7 43.21	29 42 14.7	-0.2	0.5	0.79	234.73	Q				0
53W005	17 13 22.37	50 31 42.8	-0.4	0.6	0.49	43.69	G		GR		0
53W008	17 13 47.99	49 57 36.1	-0.5	-0.2	0.85	153.41	Q		CL		0
53W009	17 13 48.90	50 24 48.6	-0.1	0.6	0.64	154.11	Q				0
53W010	17 13 50.21	50 13 37.7	0.8	-0.9	1.43	48.99	G	CM			0
53W011	17 13 50.23	49 59 3.5	2.0	0.8	2.19	8.30	G		CL		0
53W014	17 14 2.34	50 3 46.6	-0.7	-0.6	1.01	68.32	?				0
53W015	17 14 8.62	50 16 29.5	-0.4	0.2	0.72	168.81	Q				0
53W020	17 14 34.24	50 28 15.0	-0.5	-0.5	1.00	109.24	G	EL	GR		0
53W021	17 14 50.12	50 23 55.6	-0.7	-1.3	1.95	24.90	Q?		GR		0
53W022*	17 14 54.90	50 27 26.9	0.9	-4.2	2.32	2.87	Q			A	0
53W023	17 14 54.99	50 8 46.5	-1.0	0.6	1.75	41.00	G				0
53W024	17 14 55.46	50 0 1.7	0.0	-1.3	1.87	38.59	Q				0
53W025	17 15 7.87	50 20 11.3	0.5	-1.3	1.43	36.31	?				0
53W026	17 15 12.12	49 50 24.0	-0.0	-0.7	1.02	122.71	G		GR		0
53W027*	17 15 12.12	50 27 6.8	2.3	-0.4	1.18	10.64	G			B	0
53W029	17 15 14.63	50 23 33.7	-0.1	0.1	0.16	216.36	Q				0
53W030	17 15 27.88	50 12 50.8	0.2	-1.8	2.13	15.42	G		DB		0
53W031	17 15 30.69	49 59 54.1	-0.7	0.3	1.26	113.89	G				0
53W032*	17 15 31.08	49 51 57.6	-1.4	4.4	0.96	3.61	G	EL			0
53W034*	17 15 38.94	50 3 44.3	-2.8	4.8	2.25	1.57	G			B	-1
53W035	17 15 41.04	50 21 49.6	0.2	0.1	0.25	164.86	?				0
53W036	17 15 42.38	50 32 13.1	-0.9	-0.7	1.62	48.31	Q?				0
53W039	17 15 47.49	50 28 39.4	0.2	2.4	2.78	2.99	G	EL	CL		0
53W044	17 16 21.53	50 6 11.5	0.2	1.6	1.70	30.06	G	EL			0
53W045	17 16 26.71	50 18 50.6	-0.8	1.3	1.58	32.62	G	CM			0
53W046	17 16 38.26	50 10 57.5	-0.9	-1.4	2.08	18.69	G				0
53W047	17 16 53.49	50 25 49.5	-0.1	-0.3	0.51	181.29	G	CM	DB		0
53W048	17 16 56.85	50 27 5.8	0.3	-0.5	0.69	109.34	G	CM			0
53W051	17 17 14.14	49 51 24.9	0.5	11.2	15.82	0.0	Q		GR	E	-1
53W052	17 17 18.66	50 1 53.7	0.3	2.5	3.88	0.14	G		GR	D	-1
53W058	17 18 3.28	50 0 41.4	3.0	6.5	6.09	0.0	G	SP		C	-1
53W061	17 18 11.29	49 46 58.6	-0.7	0.6	0.87	68.79	Q?				0
53W062	17 18 16.62	50 2 5.2	-1.5	-0.4	1.39	29.17	G		CL		0
53W065	17 18 24.37	50 0 37.6	1.9	-0.1	2.90	3.56	G	FZ			0
53W068	17 18 43.28	49 39 6.2	0.0	0.4	0.39	157.87	?				0
53W071	17 18 56.89	50 20 13.2	0.8	-2.4	2.18	10.53	G	FZ			0
53W072	17 19 15.28	50 25 32.5	0.4	1.9	1.40	30.78	G	SP			0
53W075	17 19 26.37	49 46 42.7	-0.5	-0.0	0.73	212.16	Q				0
53W076	17 19 39.75	49 42 55.4	0.9	-1.2	1.43	43.27	G	CM			0
53W077	17 19 45.53	49 51 26.6	-11.3	-2.4	10.26	0.0	G			B	-1
53W078	17 20 3.12	50 6 26.3	1.1	-3.0	1.98	8.39	G		GR		0
53W079	17 20 8.00	50 13 22.0	-0.2	1.2	1.69	67.22	G	CM			0
53W080	17 20 22.07	49 58 26.8	-0.1	2.5	3.50	0.62	Q		CL	D	-1
53W083	17 20 33.81	50 5 28.9	0.6	-0.3	0.99	175.63	G	FZ			0
53W085	17 20 37.04	49 57 23.2	-0.2	0.7	0.91	136.84	Q	FZ			0
53W086	17 20 42.15	49 56 22.5	-3.5	0.7	3.43	0.23	G	FZ		D	-1
53W090	17 21 8.67	49 59 30.3	-1.7	1.0	1.90	18.68	G	SP		2	0
54W008	0 13 16.40	15 48 42.3	-2.2	-16.6	1.49	1.90	G	SP		C	-1
54W009*	0 13 20.70	15 58 18.1	-2.7	-2.2	1.75	4.23	G	CD	GR	7	0
54W013	0 13 39.76	16 11 28.6	-0.6	-0.6	0.62	36.82	G	PC		3	0
54W014	0 13 40.16	15 34 41.2	-1.0	-0.9	1.52	40.21	?				0
54W017*	0 13 49.34	15 41 44.1	-2.7	4.6	1.34	3.65	G	CM	CL		0
54W018	0 13 49.84	15 53 30.4	4.4	-3.2	4.76	0.00	G	SP		C	-1
54W021	0 13 52.37	16 4 22.1	0.8	1.2	1.13	41.59	G	CM	GR		0
54W028	0 14 5.99	15 51 52.3	1.0	0.2	1.81	67.96	G	EL			0
54W034	0 14 20.62	16 7 5.3	1.6	-7.7	3.61	0.13	G	PC		C	-1
54W036	0 14 26.15	15 22 53.5	1.1	-2.5	1.90	17.18	G				0
54W038	0 14 28.48	15 53 59.6	-0.4	-1.2	1.05	94.06	G				0
54W039	0 14 29.19	15 26 35.3	0.9	-1.0	1.43	53.29	G				0
54W048	0 14 55.53	16 32 22.2	0.5	-2.2	1.47	46.11	Q				0
54W049	0 14 59.55	16 38 48.9	-3.5	0.6	3.43	0.10	G			E	-1
54W050	0 15 0.34	15 12 47.8	0.9	-0.4	1.51	58.00	G		CL		0
54W052	0 15 5.71	15 54 26.3	-0.4	0.6	0.90	184.43	G				0
54W053	0 15 6.13	15 30 55.8	0.7	-6.3	3.35	0.43	G		DB	D	-1
54W057	0 15 9.52	16 34 36.8	0.4	0.8	1.13	154.94	G?				0
54W058	0 15 14.46	15 23 5.0	0.5	4.0	1.63	22.92	G				0
54W065	0 15 31.71	16 19 16.0	1.8	-0.8	2.36	5.42	G		CL		0
54W067	0 15 34.92	16 20 52.7	0.2	0.9	1.10	145.43	G				0
54W068*	0 15 35.01	16 32 52.7	-0.4	0.0	0.29	33.54	G		CL	5	0
54W070	0 15 41.23	15 57 6.2	-0.6	-1.5	1.21	60.99	Q?			1	0
54W071	0 15 41.66	16 29 37.0	-0.1	-1.5	0.29	22.21	?				0
54W072	0 15 42.29	16 26 45.1	2.1	1.1	2.04	5.00	G	SP			0
54W073	0 15 49.04	15 23 39.0	-0.3	3.7	1.12	28.72	Q		GR	7	0
54W078	0 15 53.80	15 14 2.3	2.3	3.2	2.34	2.28	G	CM	CL		0
54W079	0 15 56.20	16 4 3.7	-0.3	0.6	0.99	227.17	?				0
54W081	0 16 1.89	15 41 50.7	-0.4	0.5	0.71	176.49	G	FZ			0
54W084*	0 16 6.17	15 45 30.4	0.1	-5.2	1.72	11.92	G	CM			0
54W088	0 16 35.03	15 35 43.4	0.3	-3.4	2.08	14.26	G				0
55W007	8 32 5.69	45 5 50.3	0.8	-0.3	1.11	116.52	G		CL		0
55W010*	8 32 49.42	45 7 47.8	0.4	-1.1	1.02	75.31	G				0
55W016	8 33 20.06	45 16 48.6	0.7	-2.2	2.47	9.55	G	CM			0
55W017	8 33 22.12	45 23 12.9	-0.5	-0.4	0.77	161.40	G	CM			0
55W018	8 33 31.72	44 42 49.8	1.1	-0.4	1.61	79.06	Q				0
55W019	8 33 41.81	45 12 43.3	0.3	0.7	1.00	144.71	G		GR		0
55W020	8 33 42.19	45 20 22.8	-1.6	0.6	1.27	28.65	G	SP			0
55W023	8 33 48.56	45 18 17.5	-2.8	-6.4	3.96	0.03	G	CM	GR	E	-1
55W024	8 33 49.44	45 11 58.0	-0.9	-0.4	1.38	102.44	G	EL			0
55W027	8 33 55.75	45 9 0.9	-0.7	0.7	0.89	72.88	G				0
55W034	8 34 9.00	45 35 50.8	-0.7	-0.9	0.94	69.46	G				0
55W036	8 34 15.56	45 15 46.3	-0.1	0.8	1.20	142.25	G	FZ			0
55W037*	8 34 27.25	45 0 57.0	0.9	-2.7	4.41	0.02	G	EL		A	-1
55W041	8 34 46.69	44 58 57.9	0.3	-4.5	4.00	0.05	G	EL		D	-1
55W042	8 34 51.31	45 32 44.2	1.0	-0.7	1.49	71.43	G		CL		0
55W043	8 35 14.28	44 57 38.7	2.1	-1.9	3.38	0.67	G	EL		E	-1
55W044	8 35 16.19	44 58 57.8	3.7	-0.4	5.28	0.0	G	EL	CL	E	-1
55W046	8 35 24.06	45 32 8.2	-1.3	0.7	1.27	50.07	G				0
55W049	8 35 35.89	44 50 52.4	-1.4	-0.2	1.64	48.31	G	FZ	CL		0
55W056	8 35 59.21	45 18 46.5	0.8	1.5	2.24	21.68	G	EL			0
55W058	8 36 18.75	45 0 45.1	-3.3	-5.7	3.98	0.03	G		GR	B	-1
55W063	8 36 36.75	44 55 30.4	0.1	-0.8	1.20	165.46	G	CD	CL		0

TABLE IVa *(continued)*.

NAME	RA(1950) H M S	DEC(1950) D M S	DRA (")	DDEC (")	R	LR	ID	MORPH	ENVIR	NOTES	CODE
55W065	8 36 42.72	44 44 13.1	-0.5	0.6	0.67	83.66	G?				0
55W066	8 36 52.06	45 16 17.1	1.4	0.8	2.52	19.13	G				0
55W067	8 36 52.89	45 10 29.1	0.0	0.1	0.20	351.39	G			1	0
55W068	8 37 3.87	45 15 25.0	0.1	-0.2	0.17	141.39	G	CM			0
55W070*	8 37 11.87	44 42 2.4	5.4	6.3	5.60	0.0	Q			A	-1
55W075	8 37 26.64	44 50 40.4	0.5	0.1	0.77	312.68	Q				0
55W077	8 37 30.48	44 45 18.7	0.4	0.0	0.55	270.37	G	EL	DB		0
55W080	8 37 38.62	45 1 5.4	-6.2	3.2	9.92	0.0	?	FZ		B	-1
55W092	8 38 13.33	45 6 55.9	0.7	-2.0	1.77	26.70	G				0
55W093	8 38 17.97	44 48 56.3	-1.9	-4.2	3.71	0.13	G?			E	-1
55W097	8 38 30.27	44 53 59.1	-1.4	2.6	2.41	6.13	G?		CL		0
55W102	8 38 46.87	45 4 52.9	-0.5	-0.2	0.70	254.62	G?	FZ			0
55W105	8 38 48.58	45 21 31.9	0.6	-0.5	0.76	111.50	G	EL			0
55W110*	8 39 28.31	44 44 58.4	0.6	0.6	0.85	97.51	Q				0
55W111	8 39 28.50	45 14 11.3	0.1	-0.9	0.72	91.79	?		GR		0
55W116	8 40 16.81	44 50 15.9	-2.8	-0.4	2.55	4.60	G				0
55W118	8 40 22.92	44 46 40.4	2.7	4.8	3.89	0.04	Q			1	-1
55W121	8 40 40.25	44 42 11.5	0.1	-0.3	0.27	83.21	Q				0
55W124	8 40 50.99	44 49 45.0	-0.1	-0.3	0.49	215.21	Q				0
55W125	8 40 52.12	44 22 8.9	1.2	1.3	2.34	14.95	Q?				0
55W127	8 41 3.36	44 54 1.7	1.3	0.2	1.46	57.13	S				0
55W129	8 41 8.69	44 40 37.9	-0.1	-1.1	0.82	61.42	G				0
55W135	8 41 17.73	44 32 31.2	0.1	0.2	0.22	176.49	G	SP			0
55W137	8 41 22.84	44 55 32.2	0.7	-0.2	0.85	125.71	G	SP		6	0
55W144	8 41 53.92	45 12 11.2	0.9	0.6	0.95	59.06	G		DB		0
55W149	8 42 2.86	45 6 22.6	0.1	0.1	0.19	215.51	G	EL	GR		0
55W150	8 42 5.38	45 1 34.1	-0.0	0.1	0.05	85.78	G		CL		0
55W153	8 42 8.31	45 7 8.3	0.5	3.8	1.85	7.19	?				0
55W154	8 42 17.48	44 51 9.4	-1.6	0.9	2.33	14.79	G	CM	CL		0
55W157	8 42 40.57	44 56 50.8	-0.5	-0.5	0.66	86.87	Q				0
55W158	8 42 41.19	44 41 52.6	-2.8	-1.0	2.60	2.78	G				0
55W160	8 42 44.87	44 47 45.8	-0.3	3.2	2.45	4.38	?				0
55W161*	8 43 4.03	44 40 57.0	-2.6	0.5	0.59	4.45	G	CM		5	0
55W163	8 43 5.15	44 28 46.5	1.8	-0.6	2.15	14.14	Q			6	0
55W164	8 43 7.71	44 45 9.2	2.4	-1.9	2.23	5.59	Q				0
55W165*	8 43 12.65	44 52 46.2	0.0	-3.0	2.27	6.98	Q?			5	0
55W166	8 43 12.72	44 41 54.0	0.2	-0.4	0.54	164.38	G				0
55W171	8 43 43.31	44 33 46.9	0.4	0.1	0.52	208.83	G	CM			0
55W173	8 43 57.36	44 49 46.0	0.4	0.3	0.69	190.70	Q				0
55W175	8 44 10.58	44 15 13.2	0.5	0.4	0.93	189.82	G		GR		0
55W178	8 44 21.05	44 45 52.6	0.9	0.1	0.73	58.42	G	SP			0
55W179	8 44 21.61	44 37 15.2	1.0	-0.0	1.38	113.00	Q				0
55W183	8 44 37.71	44 44 10.0	0.6	-0.6	0.48	36.95	G	SP		C	0
55W184	8 44 39.48	44 39 35.0	0.2	0.3	0.20	61.16	G?				0
55W187*	8 44 55.08	44 24 25.7	-1.6	2.2	2.22	8.79	G	EL		A	0
55W188	8 45 3.00	44 51 35.2	-0.9	-0.3	1.30	134.79	G?			1	0
55W189	8 45 12.44	44 10 28.0	-3.2	1.9	1.98	4.60	Q?				0
55W190	8 45 14.19	44 40 47.6	-0.7	-0.5	1.06	128.46	G?		GR		0
55W191	8 45 16.35	44 13 4.4	2.6	-0.8	2.47	7.64	G		CL	3	0
55W198	8 45 40.39	44 39 8.6	0.1	0.1	0.07	100.54	Q?			1	0
55W199	8 45 42.90	44 32 28.9	0.4	-1.4	1.48	45.39	G?				0
55W200	8 45 43.71	44 13 35.2	1.7	1.5	2.04	14.74	G	CM			0
55W209*	8 46 5.62	44 39 47.1	0.4	0.1	0.33	94.15	G		CL	B	0
55W210	8 46 12.56	44 32 42.4	-0.4	-1.8	1.49	31.97	G		CL		0
55W222*	8 47 14.87	44 20 7.6	-4.0	-9.4	2.79	0.44	Q?			E	-1
55W224*	8 47 30.14	44 48 59.7	-1.9	0.5	2.32	14.79	Q				0
55W226	8 47 35.74	44 34 40.3	0.8	-1.2	1.63	48.18	G				0

TABLE IVb. — *The list of identifications NOT in a complete sample.*

NAME	RA(1950) H M S	DEC(1950) D M S	DRA (")	DDEC (")	R	LR	ID	MORPH	ENVIR	NOTES	CODE
52W009	13 5 12.75	29 20 43.3	-2.0	1.3	1.73	12.29	Q?				2
52W029	13 6 21.34	29 14 17.9	-0.6	-1.1	1.25	87.07	?				1
52W036	13 6 50.03	29 40 26.9	1.0	-0.5	1.03	46.86	G	IR	DB	C	2
52W042A	13 7 10.31	29 34 47.4	0.4	0.9	1.43	111.28	?			5	2
52W046	13 7 32.44	29 48 24.0	1.5	2.9	2.28	5.94	?				1
52W052	13 8 20.65	29 39 55.6	2.3	-5.2	1.69	4.23	Q				2
53W003	17 13 1.98	50 21 38.6	1.0	-4.6	2.44	1.88	G	SP	DB	C	2
53W028	17 15 13.43	50 39 46.6	-0.6	-1.3	1.23	35.71	G				2
53W067	17 18 36.37	50 13 55.6	1.2	-0.5	2.17	36.34	?				1
54W005*	0 12 52.85	16 33 27.9	-2.2	1.7	1.25	7.29	G?				2
54W025	0 14 1.52	15 10 30.7	-1.6	0.6	2.58	6.82	Q?				2
54W032	0 14 16.41	16 42 2.4	-0.4	10.4	2.55	1.58	G	CM		2	2
54W040	0 14 29.37	16 22 25.5	-0.1	-6.0	1.33	21.24	?				1
54W044	0 14 37.98	15 50 2.7	1.6	-3.1	1.68	8.93	Q				2
54W047	0 14 53.07	16 23 14.2	-0.2	5.8	1.42	14.11	Q				2
54W056	0 15 9.04	15 37 28.6	-3.9	-0.1	1.53	1.60	G		GR		2
54W059	0 15 16.48	15 39 28.6	1.4	5.9	2.77	2.14	?				1
54W068A	0 15 34.50	16 32 38.6	-2.0	1.6	2.99	1.41	G?		CL	5	2
54W068B	0 15 35.89	16 32 60.0	-0.8	5.2	1.43	11.33	G		CL	5	2
54W069	0 15 39.53	16 26 53.9	0.1	5.5	2.68	4.51	?	FZ			1
54W089	0 16 52.91	15 39 15.3	0.7	1.4	1.19	45.73	Q				2
55W009	8 32 40.58	44 54 4.2	1.3	-0.8	1.19	38.11	G	SP		C	2
55W014	8 33 15.81	45 20 12.4	-2.0	0.5	2.00	15.44	?		CL		1
55W037A	8 34 26.40	44 59 57.8	-0.1	-1.5	2.28	14.97	?	PC		5	2
55W037B	8 34 27.90	45 1 39.6	3.0	9.5	15.49	0.0	?	PC		5	2
55W052	8 35 44.56	45 12 53.1	-2.8	0.0	2.00	7.82	G				2
55W074	8 37 18.21	44 54 8.1	-2.6	1.0	1.43	12.24	Q				2
55W096	8 38 28.00	45 4 0.8	-2.8	-1.2	2.40	4.33	?				2
55W131	8 41 11.81	44 56 55.4	-1.6	-0.4	1.45	27.86	?				1
55W136	8 41 21.31	44 43 18.2	1.5	0.3	1.44	35.64	?		CL		1
55W152	8 42 6.94	45 9 51.6	5.3	-5.7	7.73	0.0	G	SP			2
55W161A	8 42 59.55	44 41 3.5	-0.4	12.0	9.21	0.0	Q			5	2
55W161B	8 43 4.03	44 40 57.0	0.6	2.7	0.46	4.31	G			5	2
55W165A	8 43 11.06	44 52 40.5	-2.0	-0.6	2.23	9.87	?			5	2
55W165B	8 43 14.59	44 52 53.1	-2.1	-6.7	9.06	0.0	?			5	2
55W168	8 43 33.59	44 29 49.5	-0.6	-0.2	0.43	43.15	G?				2
55W177	8 44 18.00	44 14 33.9	0.1	-0.2	0.34	223.86	?				1
55W202	8 45 44.94	44 37 2.7	2.0	1.0	2.06	18.60	?	FZ			1
55W205	8 45 53.28	44 22 34.2	-0.9	-0.0	0.69	47.56	?		CL		1
55W206	8 45 53.94	44 11 3.8	2.9	1.3	1.91	6.65	G?				2
55W207	8 45 58.19	45 1 19.3	-3.4	1.2	2.72	1.70	G		GR		2

1984A&AS...58...39W

TABLE Va. — *Identification statistics.*

Field	Area (deg^2)	NRSS on 4m	Nopt (LR>2)	Add. cand.	N_{id} (tot)	N_{id} (LR>2)	N_{contam} (LR>2)	ID %	Rel. (%)	Compl. (%)
SA57	0.677	30	12	2	13.0	12.9	1.1	43.3	92.1	99.2
Her.1	0.620	32	13	6	17.2	16.4	2.6	53.8	86.3	95.3
Her.2	0.620	38	27	1	28.2	27.0	1.0	74.2	96.4	95.7
Total Herc	1.240	70	40	7	45.4	43.4	3.6	64.9	92.3	95.6
SA68.1	0.620	28	13	2	14.2	13.4	1.6	50.7	89.3	94.4
SA68.2	0.620	29	13	3	14.4	14.3	1.7	49.7	89.4	99.3
Total SA68	1.240	57	26	5	28.6	27.7	3.3	50.2	89.4	96.9
Lynx.1	0.563	30	13	4	15.7	15.5	1.5	52.3	91.2	98.7
Lynx.2	0.563	44	23	1	22.2	22.2	1.8	50.5	92.5	99.8
Lynx.3	0.620	38	18	1	18.1	17.9	1.1	47.6	94.2	98.9
Lynx.4	0.620	33	14	5	17.5	17.2	1.8	53.0	90.5	98.3
Total Lynx	2.366	145	68	11	73.5	72.8	6.2	50.7	92.2	99.0
Conservative			146	-	142.5	138.8	7.2	47.2	95.1	97.4
Additional			-	25	18	18	7	6.0	72	100
TOTAL SAMPLE	5.523	302	—	171	—	160.5	156.8	14.2	53.2	91.7	97.7

TABLE Vb. — *Identification content.*

Field	G+G? % (n)	? % (n)	Q+Q? % (n)	All id's % (n)	CL % (n)	GR % (n)	CL+GR % (n)
SA57	31% (10)	9% (3)	3% (1)	43% (14)	9% (3)	6% (2)	15% (5)
Her.1	37% (13)	3% (1)	14% (5)	54% (19)	6% (2)	9% (3)	15% (5)
Her.2	45% (17)	8% (3)	21% (8)	74% (28)	8% (3)	11% (4)	19% (7)
Total Herc	41% (30)	6% (4)	18% (13)	65% (47)	7% (5)	10% (7)	17% (12)
SA68.1	44% (13)	3% (1)	3% (1)	51% (15)	10% (3)	3% (1)	13% (4)
SA68.2	37% (12)	6% (2)	6% (2)	50% (16)	6% (2)	6% (2)	12% (4)
Total SA68	40% (25)	5% (3)	5% (3)	50% (31)	8% (5)	5% (3)	13% (8)
Lynx.1	40% (13)	6% (2)	6% (2)	52% (17)	9% (3)	6% (2)	15% (5)
Lynx.2	23% (11)	4% (2)	21%(*) (10)	48% (23)	4% (2)	2% (1)	6% (3)
Lynx.3	35% (14)	0% (0)	13% (5)	48% (19)	8% (3)	5% (2)	13% (5)
Lynx.4	50% (18)	0% (0)	3% (1)	53% (19)	8% (3)	6% (2)	14% (5)
Total Lynx	36% (56)	3% (4)	11% (18)	50% (78)	7% (11)	4% (7)	11% (18)
TOTAL SAMPLE	38% (121)	4% (14)	11% (35)	53% (170)	8% (24)	6% (19)	14% (43)

(*) The radio star 55W127 is not included in Lynx.2

Notes to Table Va.

Col. 1 Field Name
Col. 2 Area covered by field, corrected for overlap.
Col. 3 Number of radio sources in complete sample, also within 4 m plate.
Col. 4 Number of candidate identifications with LR > 2.0.
Col. 5 Number of additional candidates, suggested for reasons mentioned in section 3b and in the notes following Table 4.
Col. 6 Expected number of real identifications amongst all radio sources.
Col. 7 Expected number of real identifications with LR > 2.0.
Col. 8 Expected number of contaminating objects with LR > 2.0.
Col. 9 Total identification percentage.
Col. 10 Reliability of the sample.
Col. 11 Sample completeness.

1984A&AS...58...39W

TABLE VI. — *Identification fraction versus flux density and apparent magnitude.*

$S_{1.4GHz}$ (mJy)	$\langle S_{1.4GHz} \rangle$ (mJy)	PSS limit (E + O) f	PSS limit (E + O) %	48" Schmidt limit (IIIaJ + IIIaF) f	48" Schmidt limit (IIIaJ + IIIaF) %	Mayall 4 m limit (U,J,F,N) f	Mayall 4 m limit (U,J,F,N) %
0.23							
	0.39	3/32	6 ± 4	8/32	21 ± 7	16/32	45 ± 9
0.65							
	1.11	5/32	15 ± 6	8/32	23 ± 7	13/32	37 ± 9
1.85							
0.61							
	0.98	8/36	18 ± 6	11/36	26 ± 7	21/36	52 ± 8
1.56							
	2.21	13/69	16 ± 4	23/69	30 ± 6	30/69	41 ± 6
3.13							
	4.42	10/69	11 ± 4	21/69	26 ± 5	42/69	56 ± 6
6.25							
	8.83	11/62	14 ± 4	22/62	31 ± 6	40/62	60 ± 6
12.5							
	17.6	5/27	15 ± 7	9/27	31 ± 9	17/27	61 ± 9
25.0							
	48.9	5/27	16 ± 7	9/27	31 ± 9	12/27	42 ±10
100.0							
	193.0	2/10	} 22	6/10	} 53	7/10	68 ±15
400.0			} ±12		} ±14		
	764.0	1/ 2		1/ 2		2/ 2	99 ± 7
1600.0							
Whole survey	~ 6 mJy	55/302	15 ± 2	102/302	30 ± 3	171/302	53 ± 3

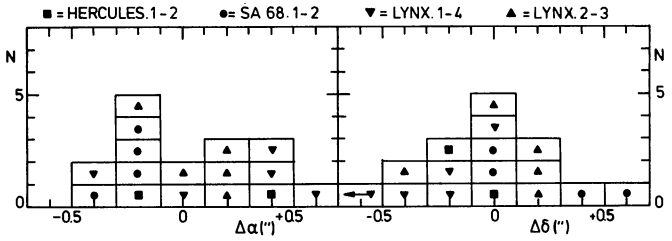

FIGURE 1. — Histogram of optical position differences for identifications found independently on overlapping plates. Systematic position errors are of order 0″.2, while random errors are about 0″.4.

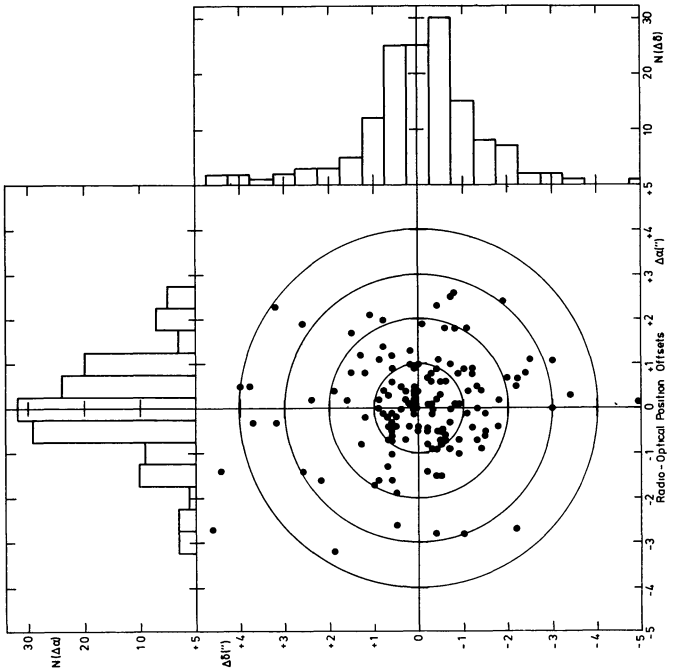

FIGURE 2b. — Vector diagram of the absolute radio-optical position differences $\Delta\alpha$ and $\Delta\delta$ for the conservative sample of 146 objects, *after* the average offsets per field (Table III) were applied.

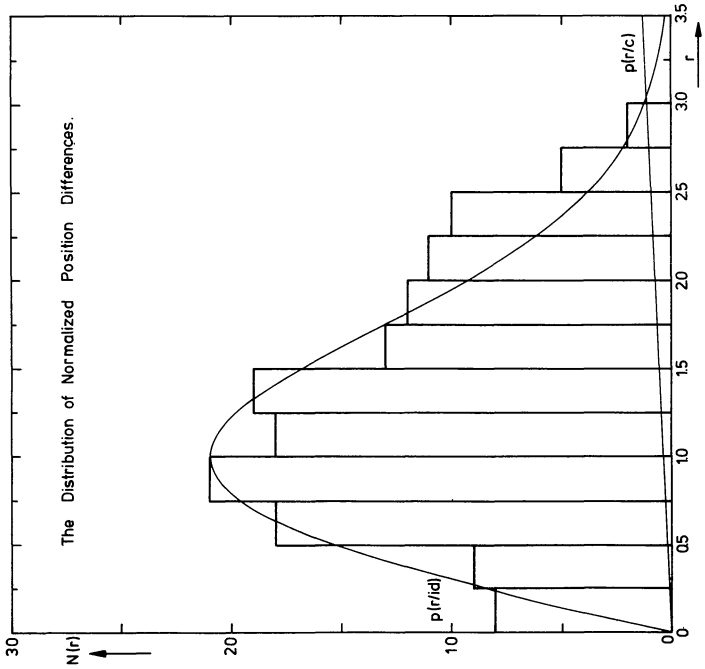

FIGURE 2a. — The distribution of normalized radio-optical position differences for all 146 objects with $LR \geqslant 2.0$. The Rayleigh distribution is shown for the expected 138.8 identifications with $LR \geqslant 2.0$, the Poisson distribution is for the expected 7.2 contaminating objects.

NE quadrant of F plate (MPF 3622) in SA57

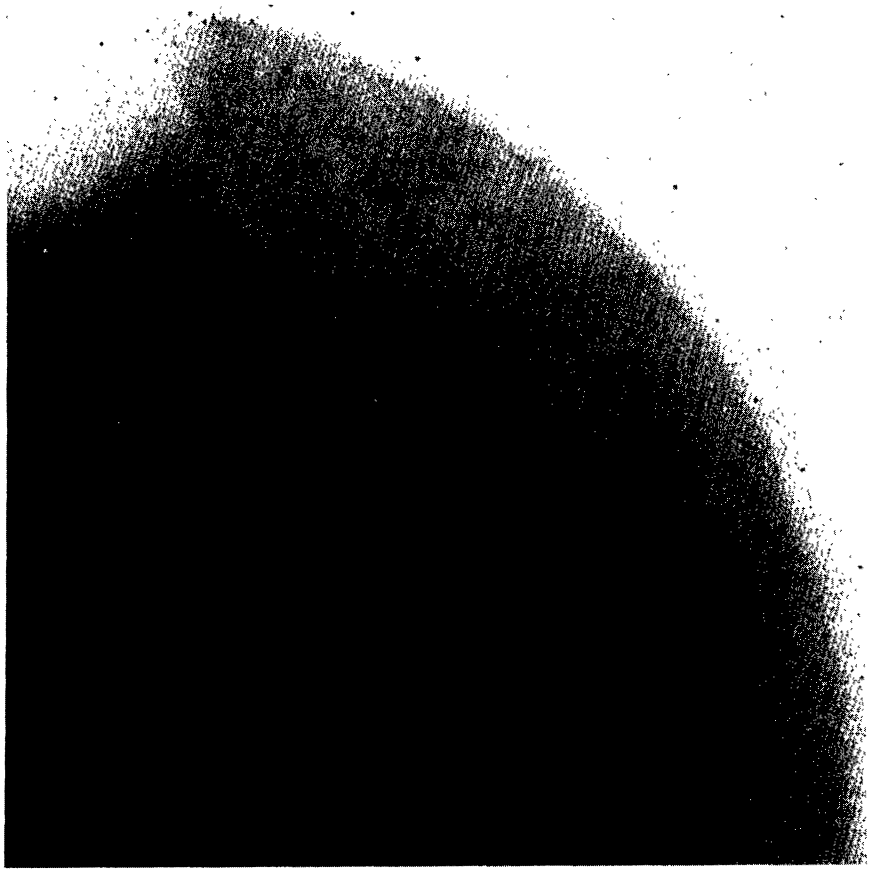

NW quadrant of F plate (MPF 3622) in SA57.

FIGURE 3. — Finding charts for the Westerbork radio source identifications prepared from the Mayall *F* plates divided in quadrants. The proposed optical identifications are marked by their Westerbork survey and source number. The finding charts are especially useful in studying the optical morphology and general environment of the radio source identifications. The 4 m plates were enlarged about 1.2 times to a scale of 16″ mm^{-1}. At the end of this paper more enlarged photo's are given for all radio source identifications in the four passbands, made from a TV display system. These are of lower dynamic range, but are more appropriate for the study of the study of the immediate surroundings of the radio sources and to visualize color differences.

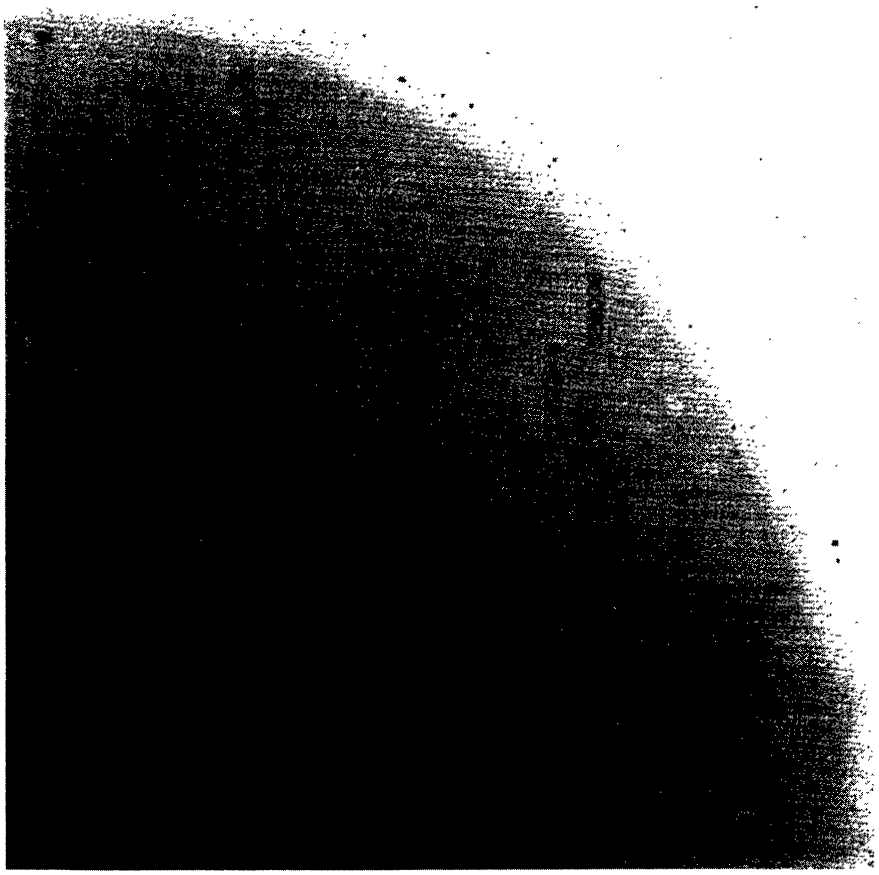

SW quadrant of F plate (MPF 3622) in SA57.

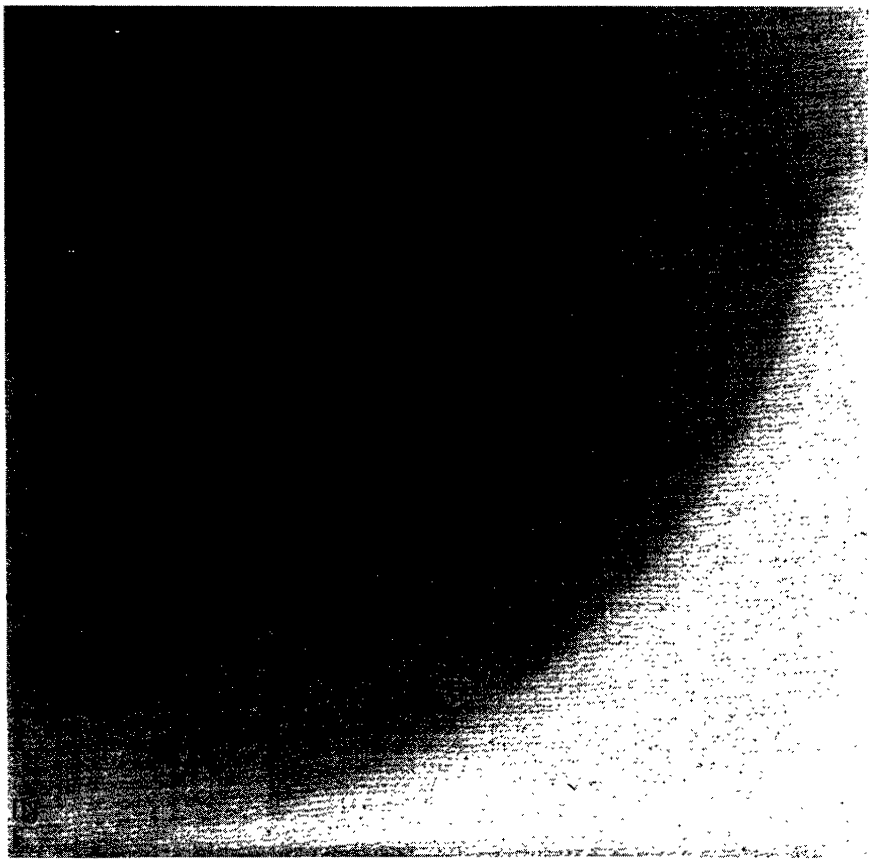

SE quadrant of F plate (MPF 3622) in SA57.

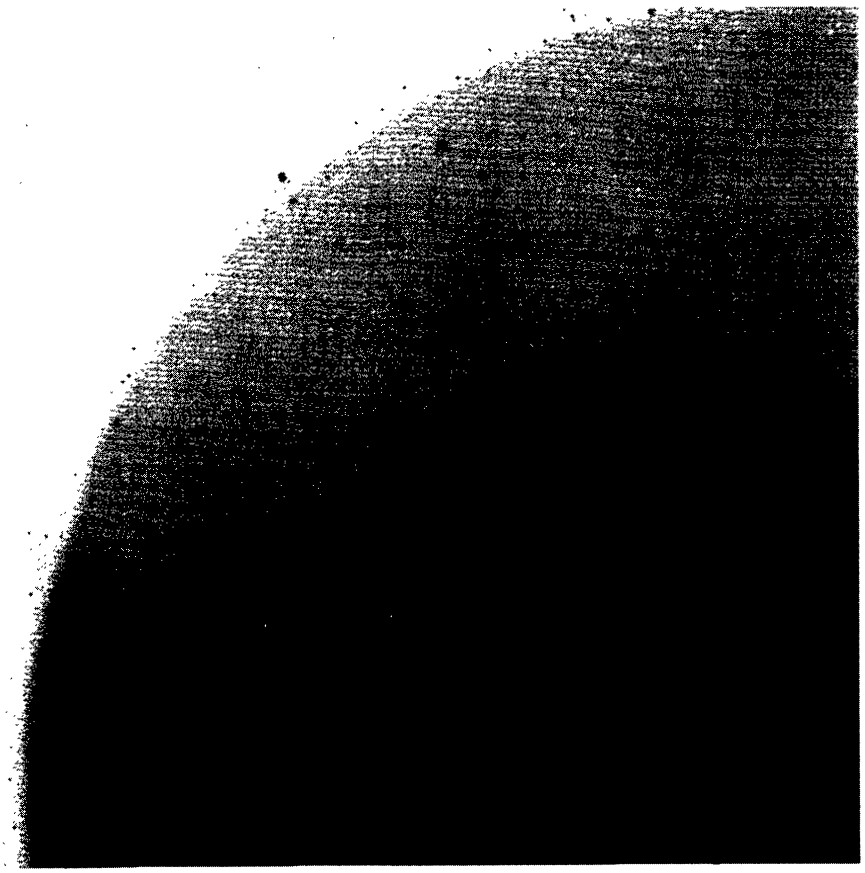

NW quadrant of F plate (MPF 1574) in Hercules.1

NE quadrant of F plate (MPF 1574) in Hercules.1

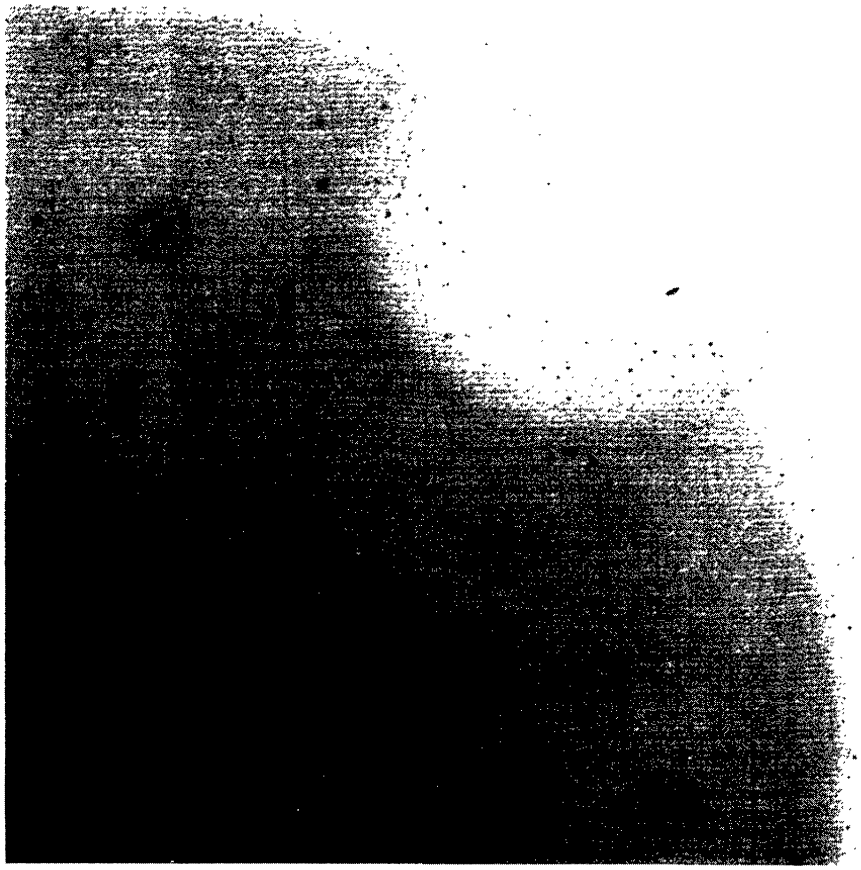

SW quadrant of F plate (MPF 1574) in Hercules.1

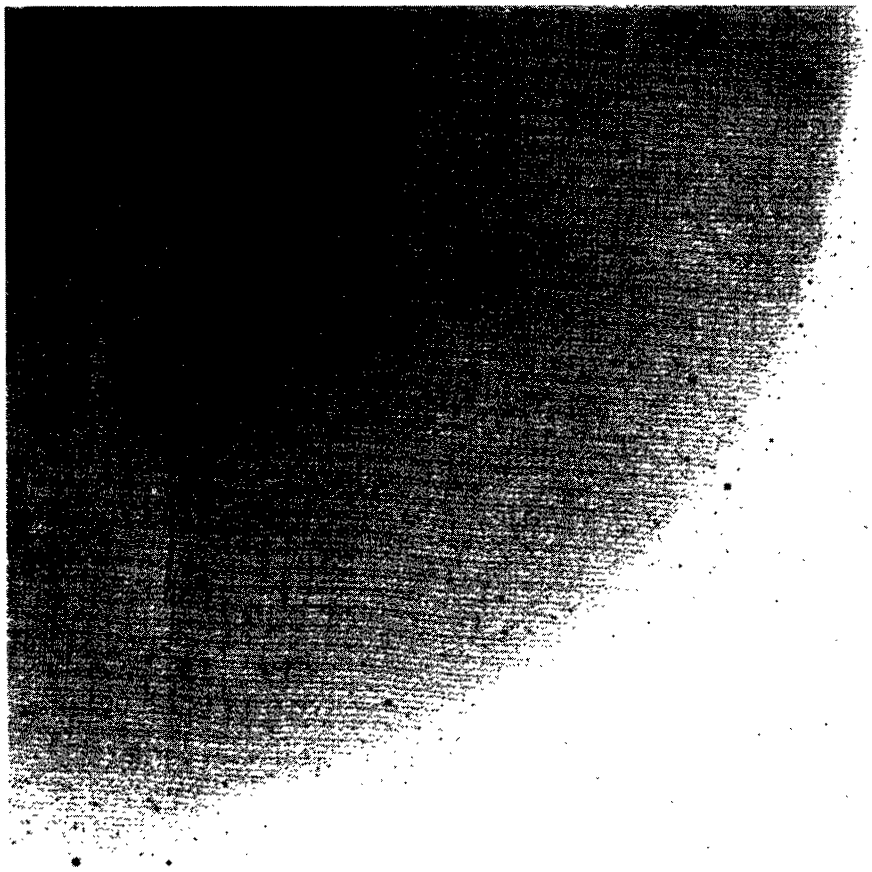

SE quadrant of F plate (MPF 1574) in Hercules.1

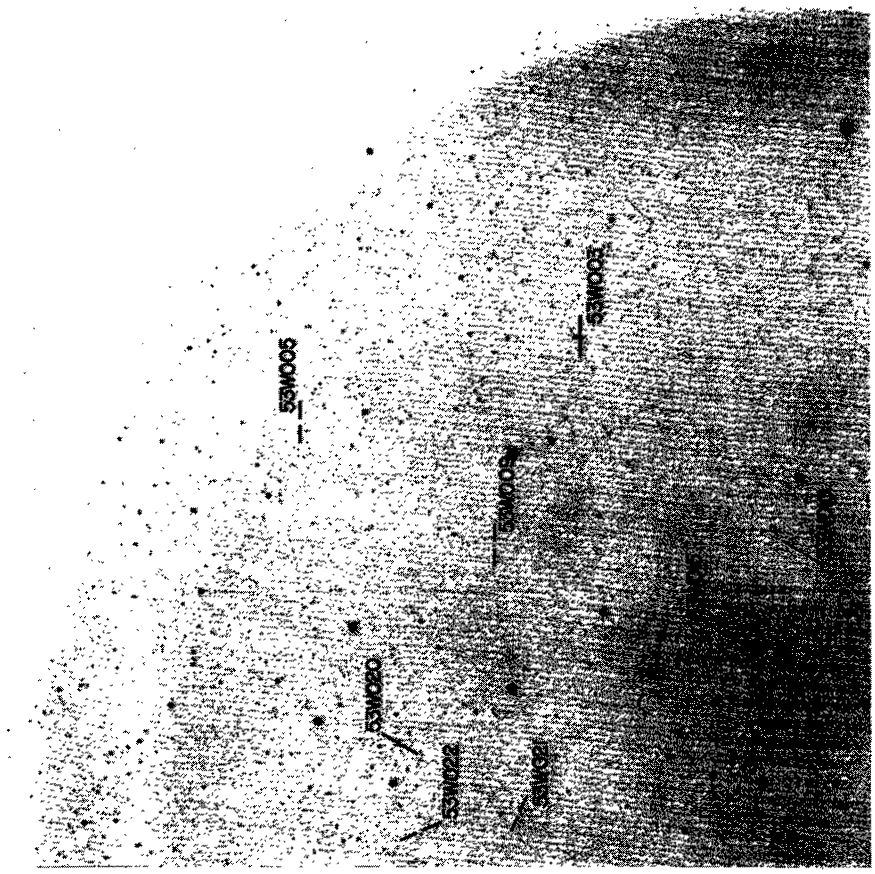

NW quadrant of F plate (MPF 1573) in Hercules.2

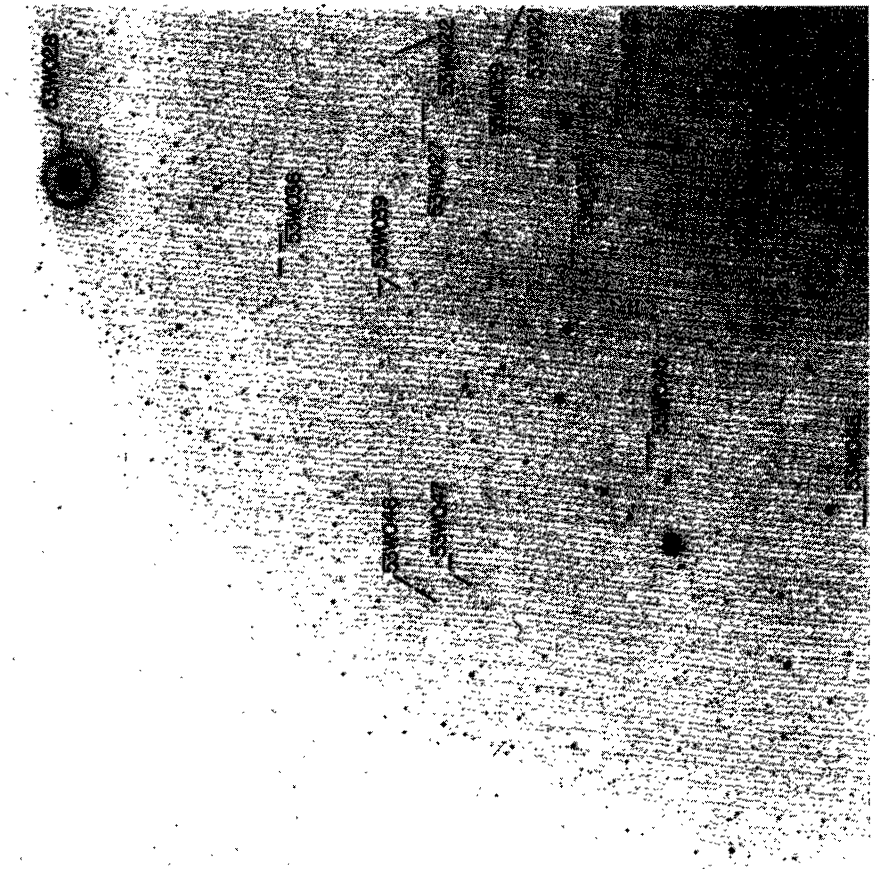

NE quadrant of F plate (MPF 1573) in Hercules.2

SW quadrant of F plate (MPF 1573) in Hercules.2

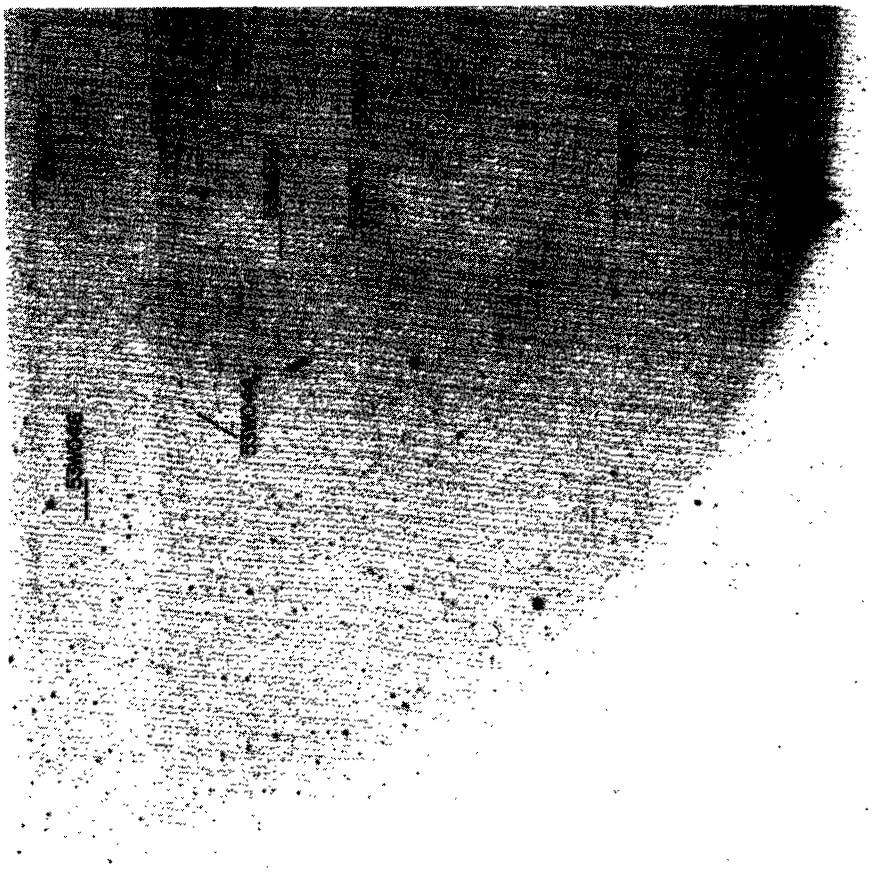

SE quadrant of F plate (MPF 1573) in Hercules.2

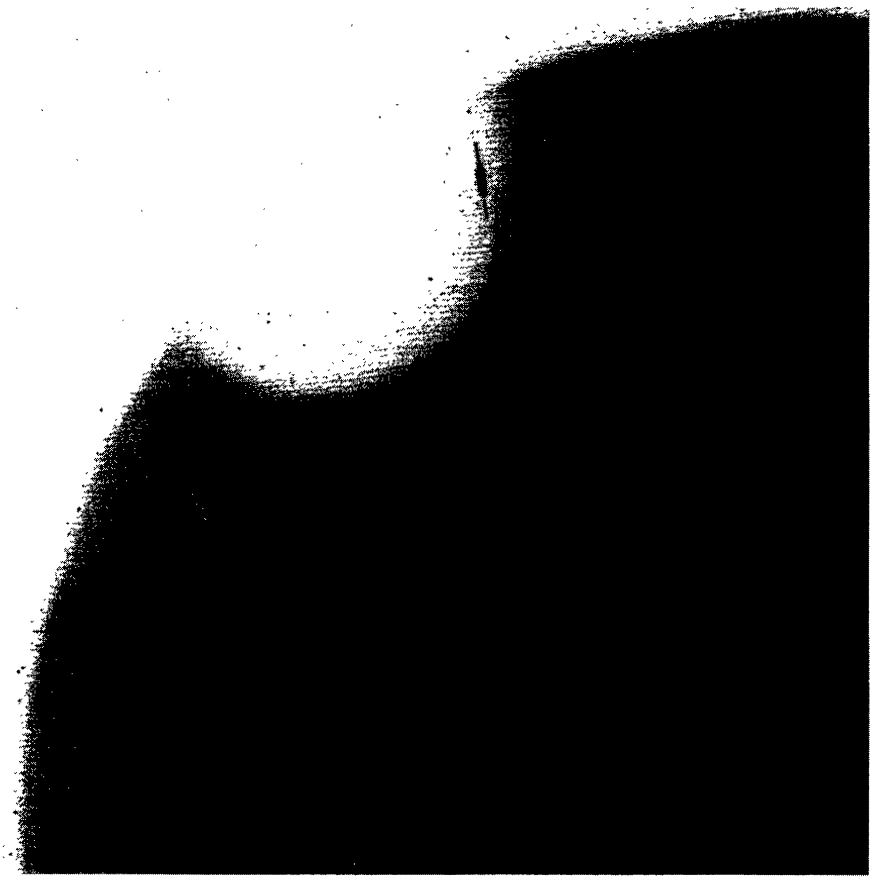

NW quadrant of F plate (MPF 1283) in SA68.1

NE quadrant of F plate (MPF 1283) in SA68.1

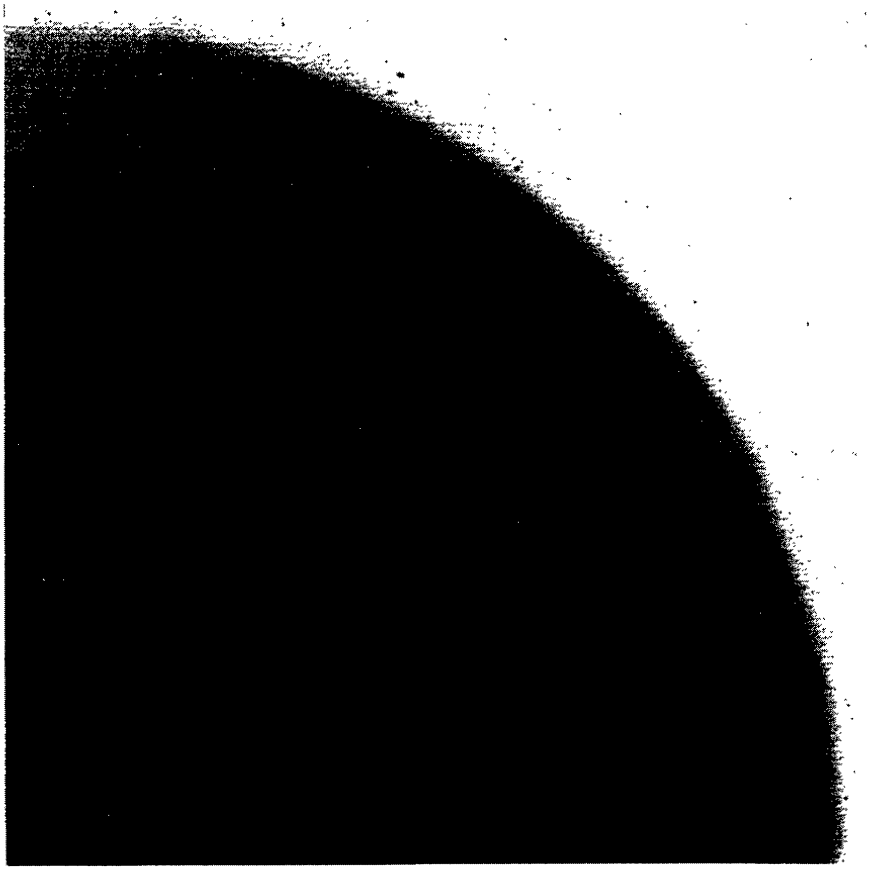

SW quadrant of F plate (MPF 1283) in SA68.1

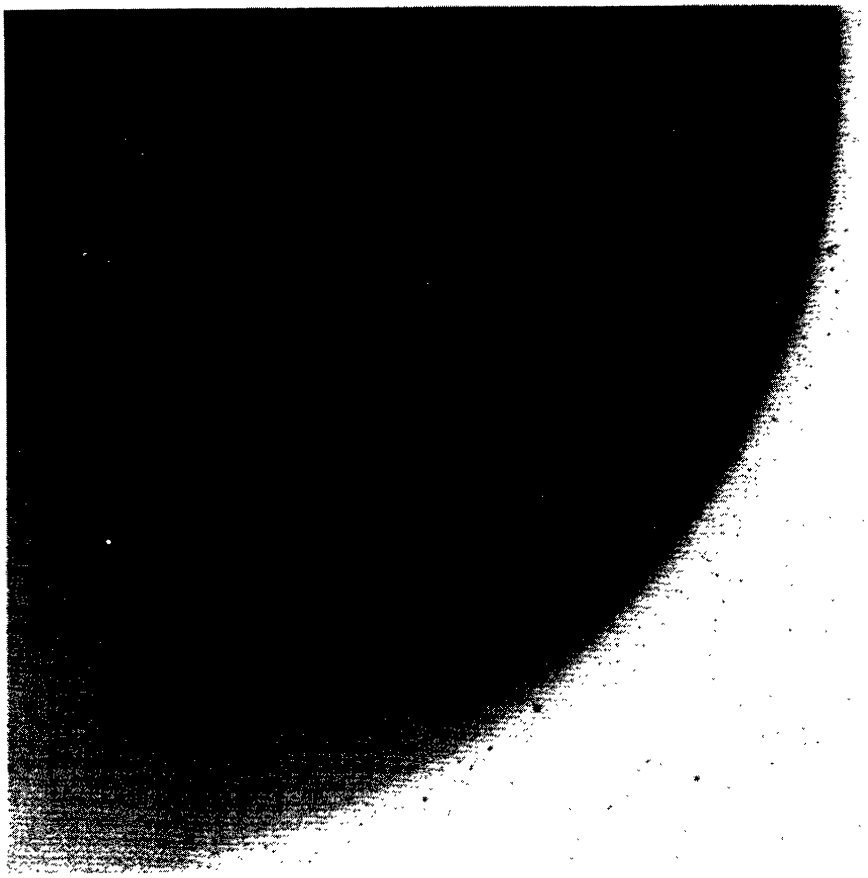

SE quadrant of F plate (MPF 1283) in SA68.1

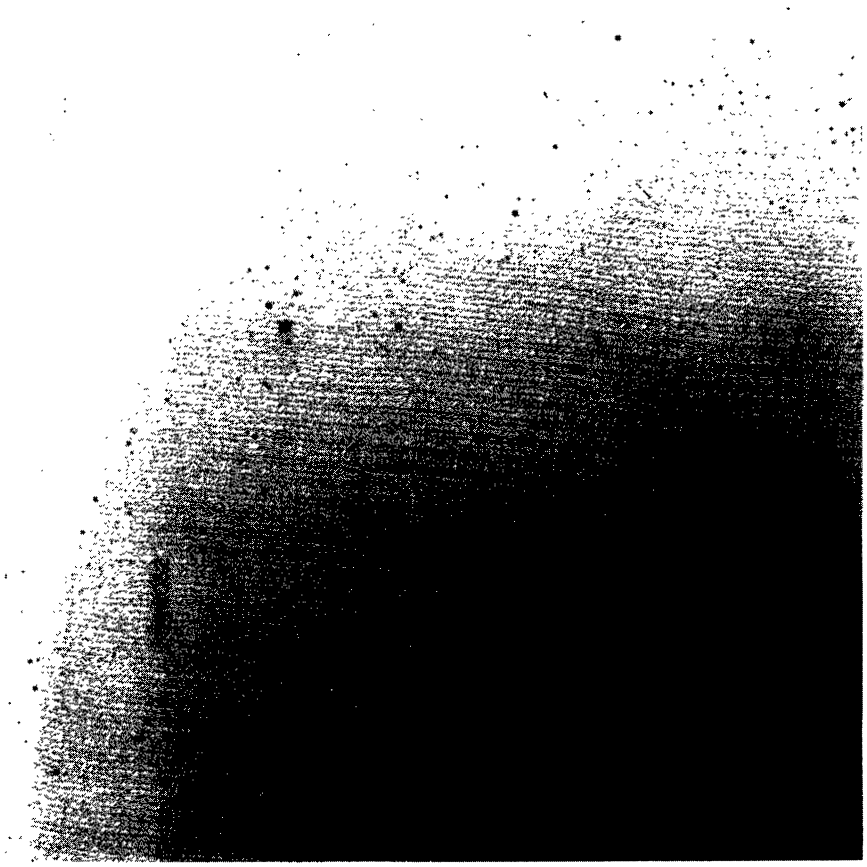

NW quadrant of F plate (MPF 1293) in SA68.2

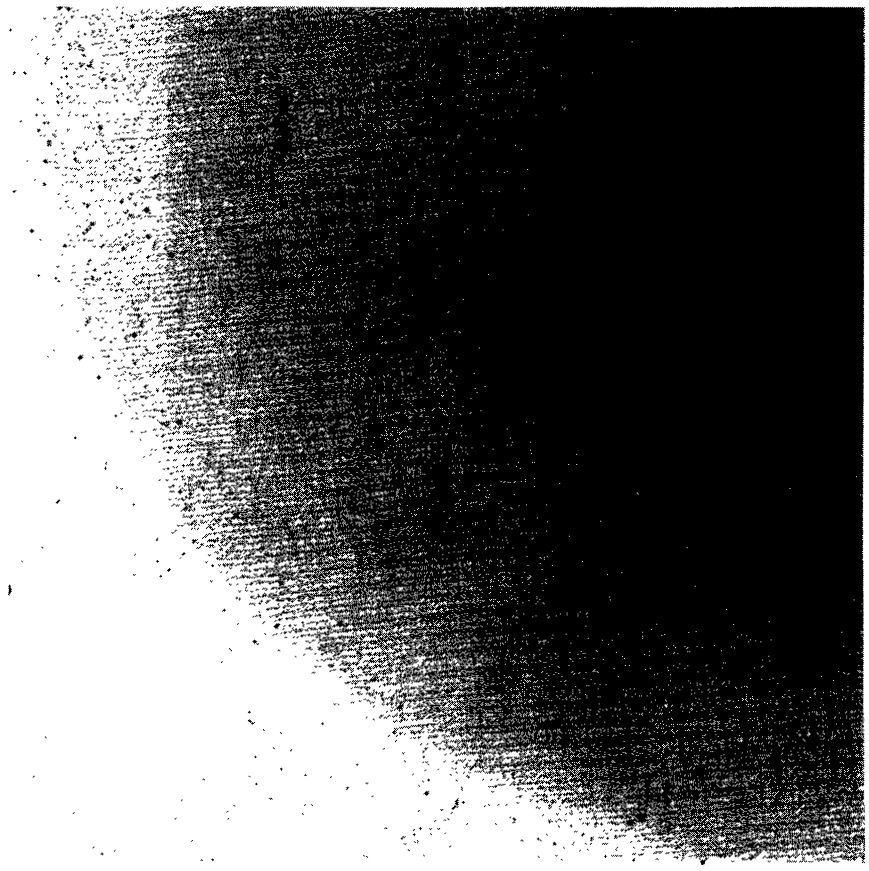

NE quadrant of F plate (MPF 1293) in SA68.2

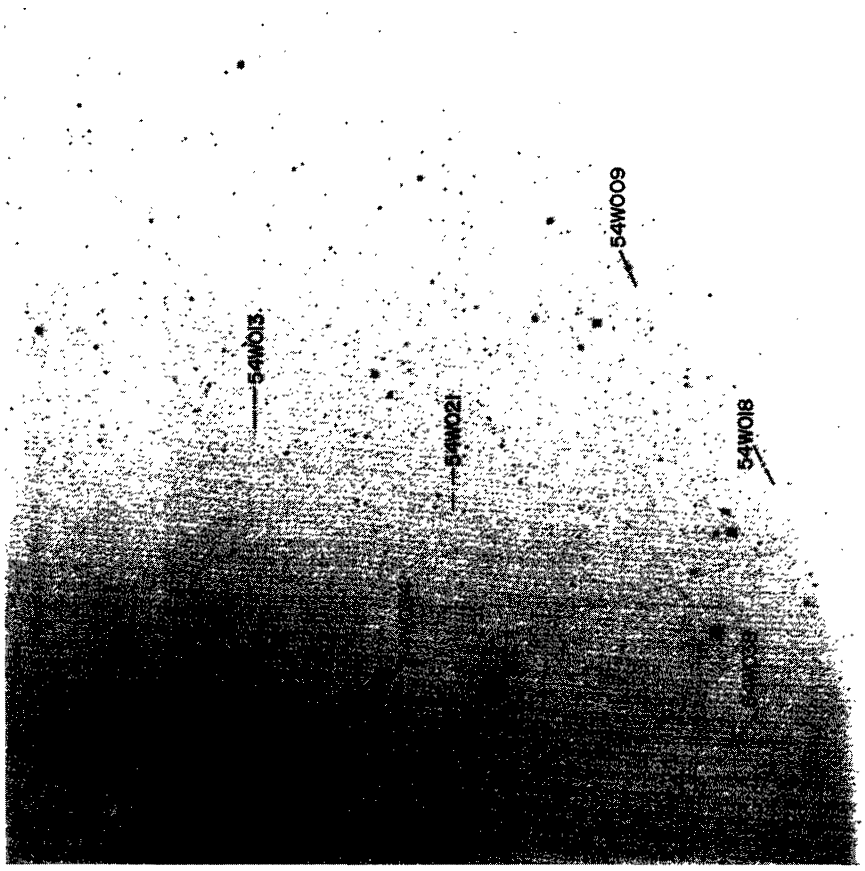

SW quadrant of F plate (MPF 1293) in SA68.2

SE quadrant of F plate (MPF 1293) in SA68.2

NW quadrant of F plate (MPF 1403) in Lynx.1

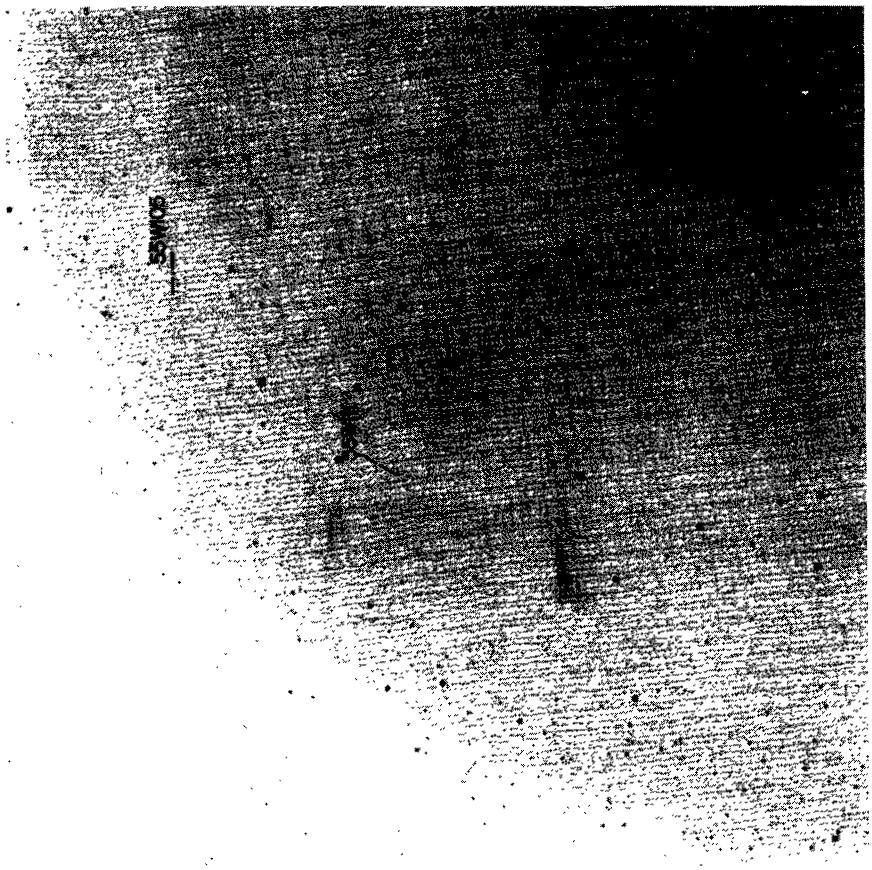

NE quadrant of F plate (MPF 1403) in Lynx.1

SW quadrant of F plate (MPF 1403) in Lynx.1

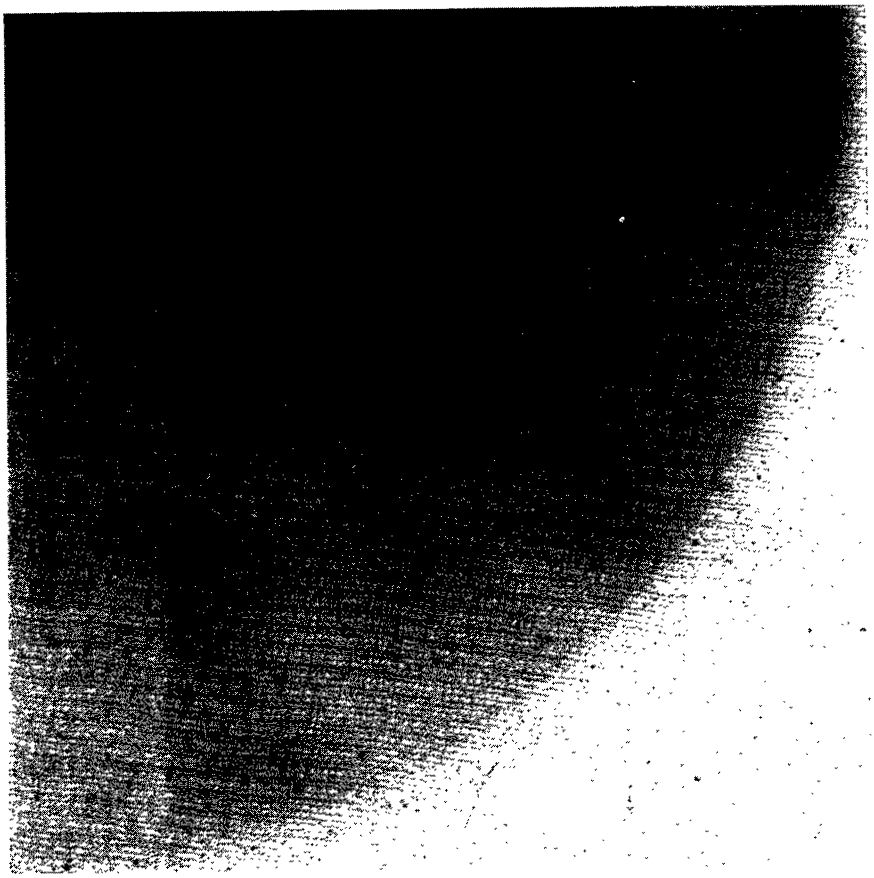

SE quadrant of F plate (MPF 1403) in Lynx.1

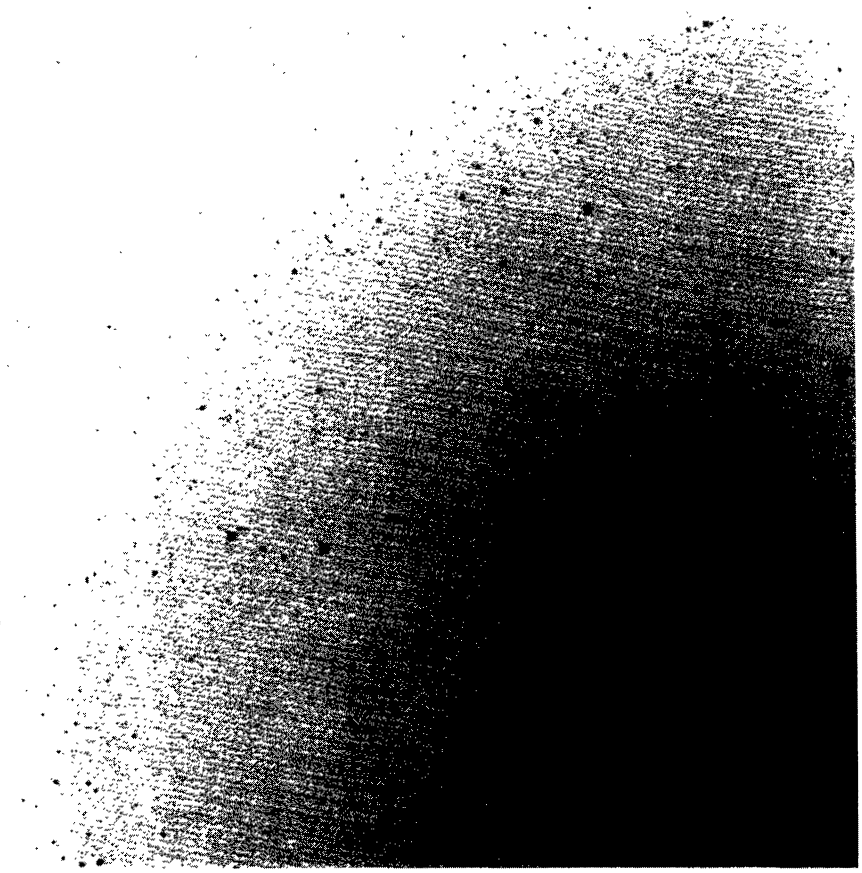

NW quadrant of F plate (MPF 1299) in Lynx.2

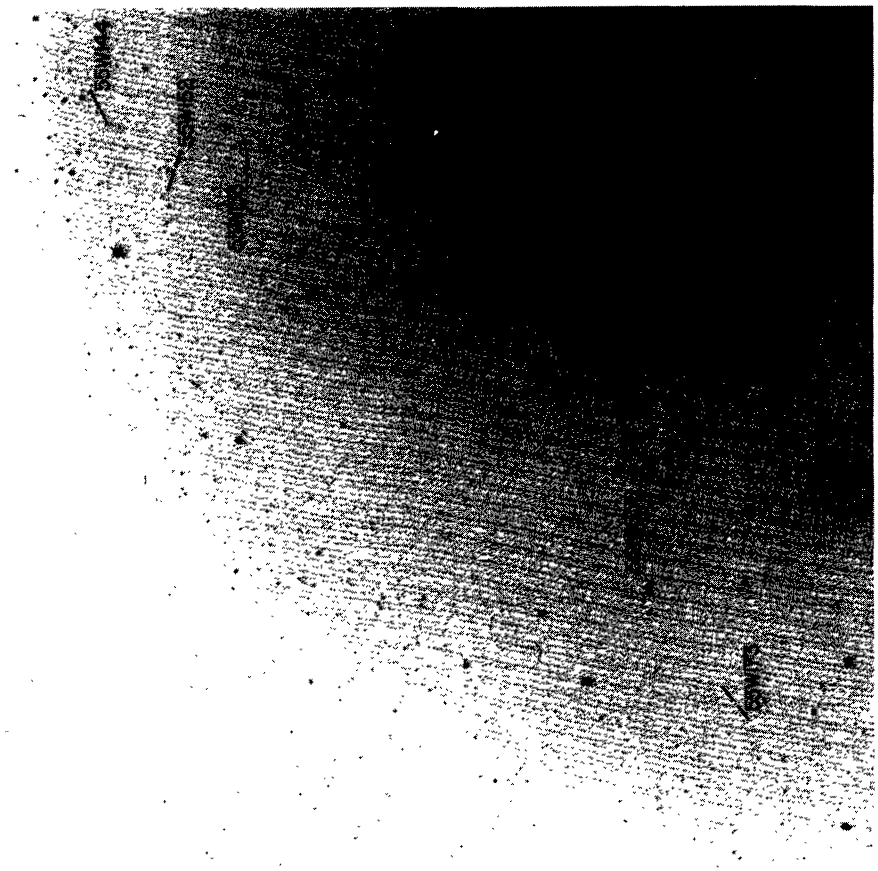

NE quadrant of F plate (MPF 1299) in Lynx.2

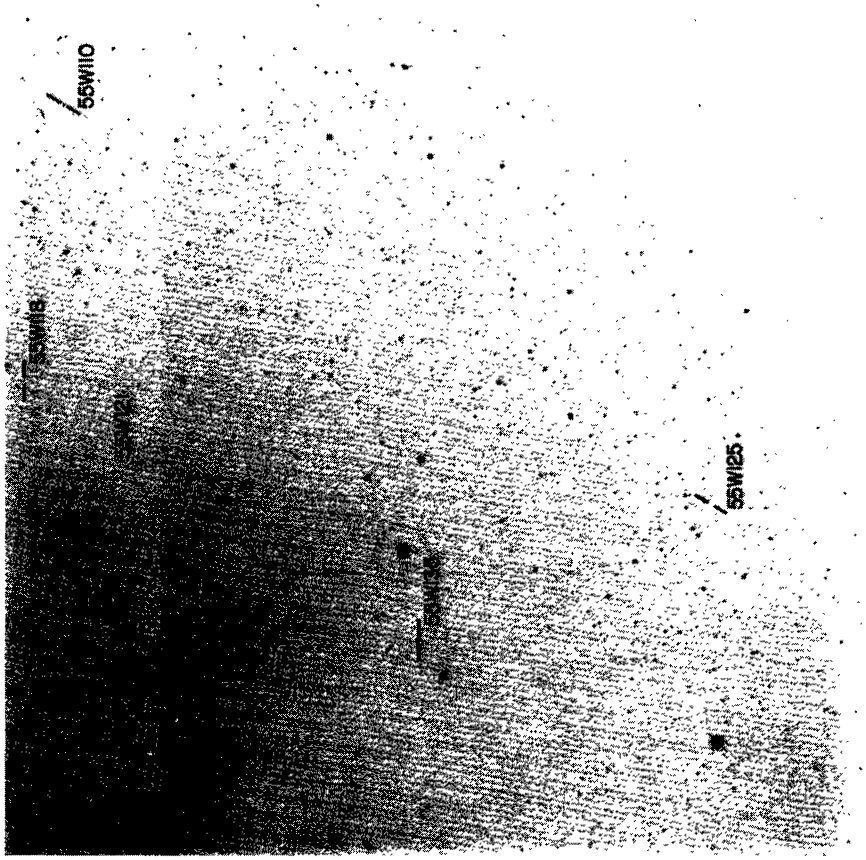

SW quadrant of F plate (MPF 1299) in Lynx.2

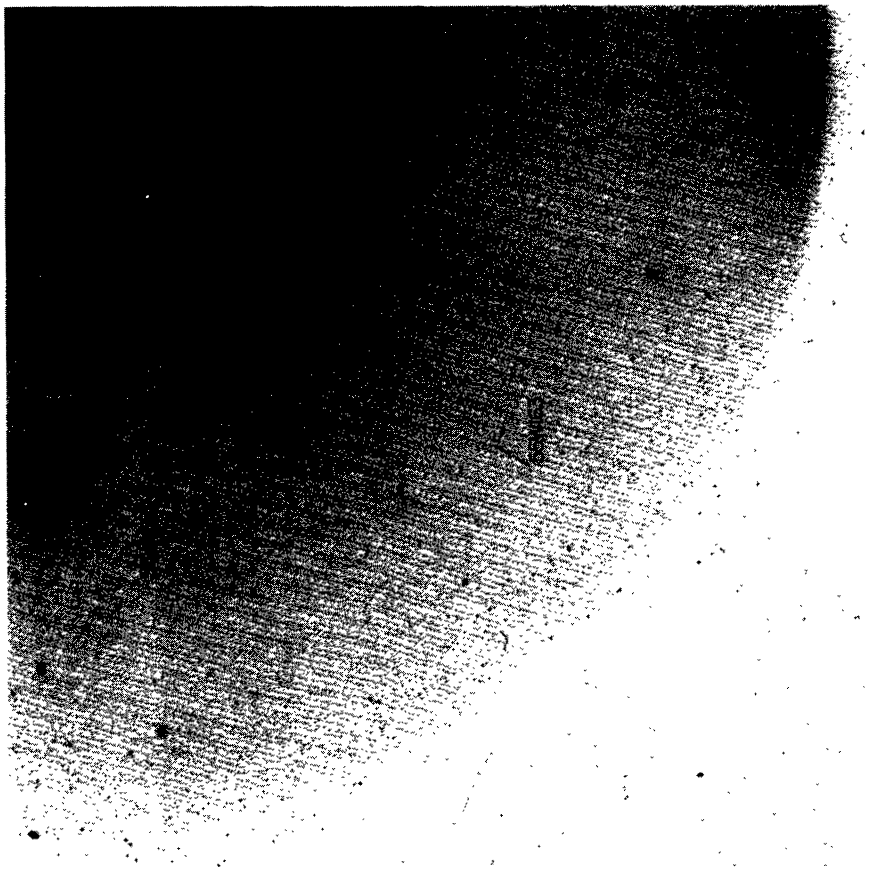

SE quadrant of F plate (MPF 1299) in Lynx.2

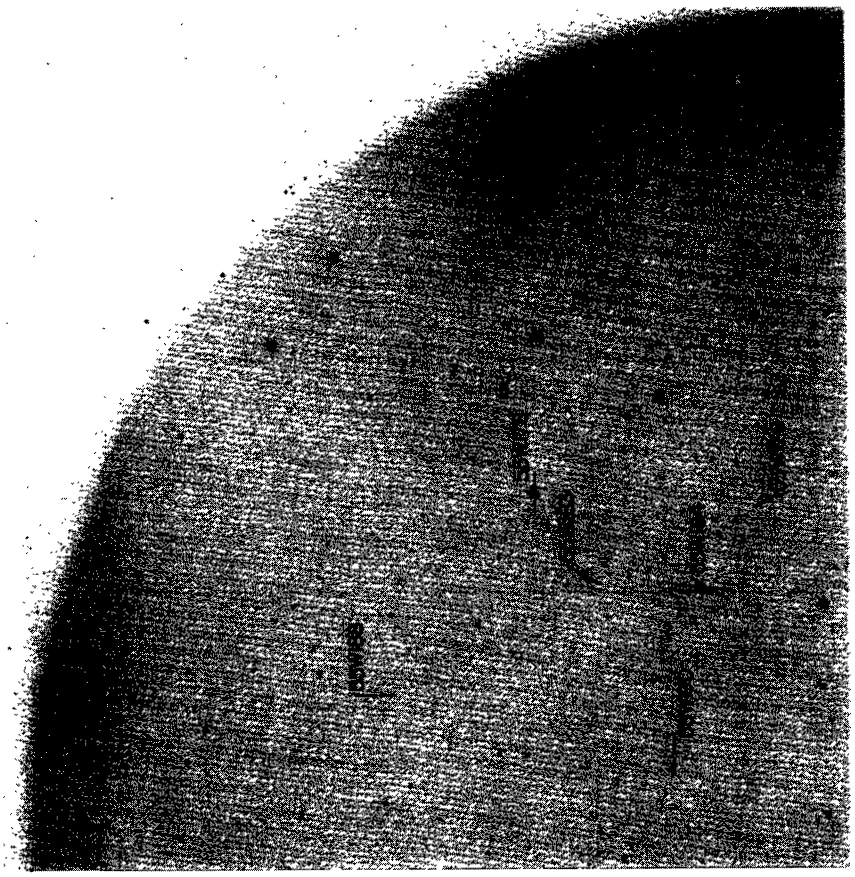

NW quadrant of F plate (MPF 1411) in Lynx.3

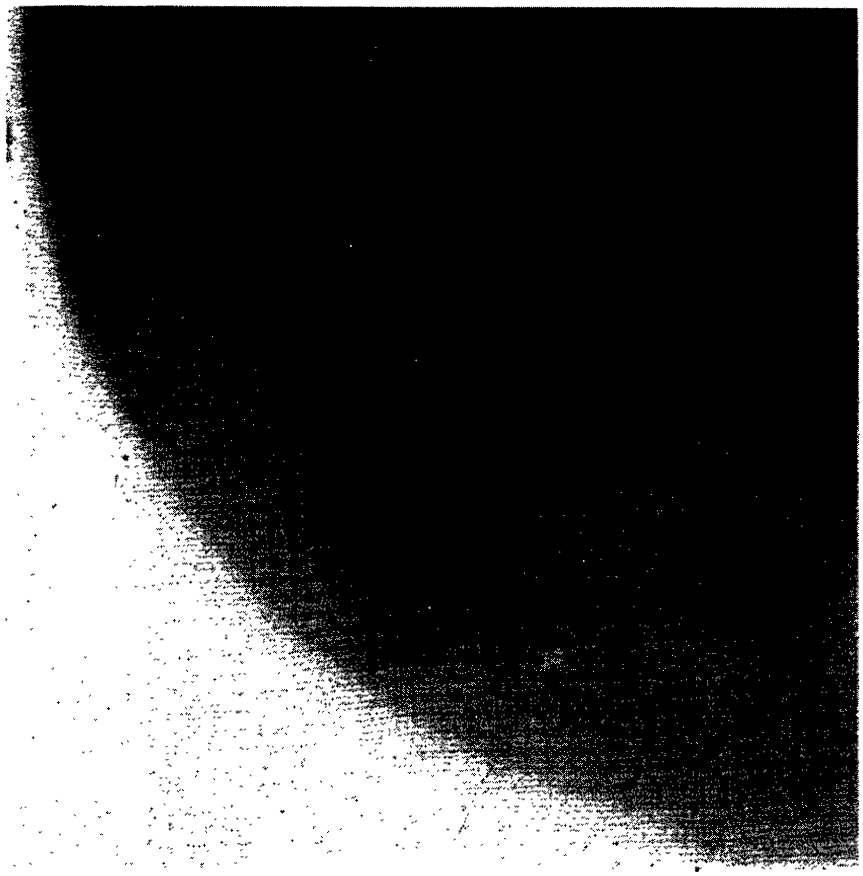

NE quadrant of F plate (MPF 1411) in Lynx.3

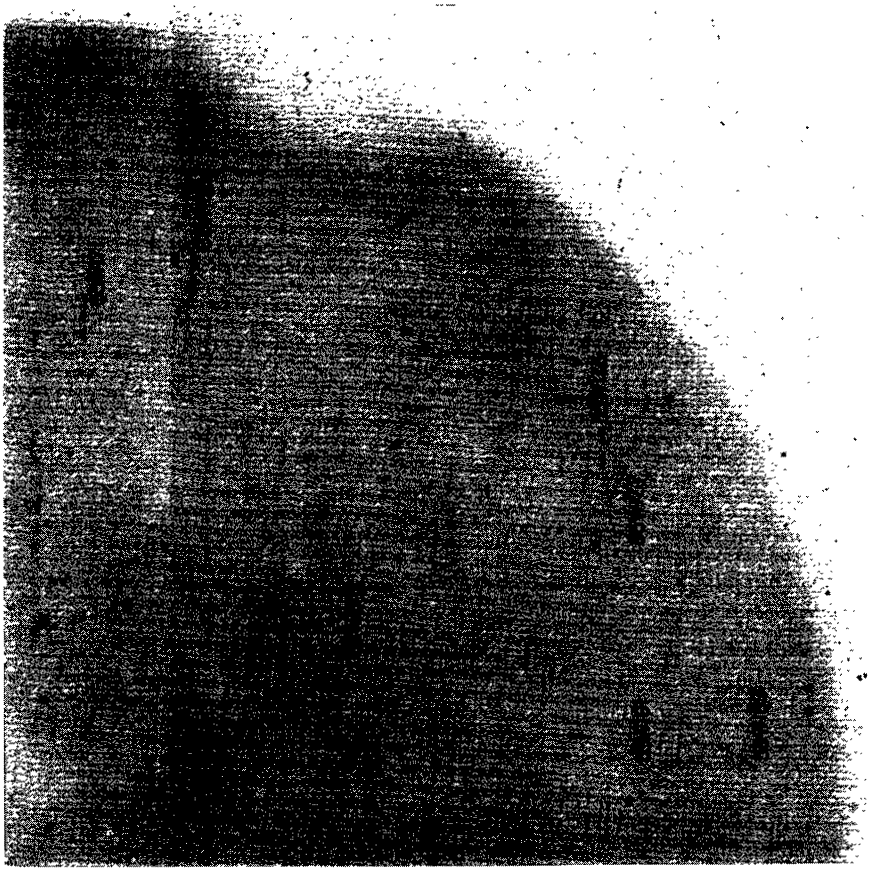

SW quadrant of F plate (MPF 1411) in Lynx.3

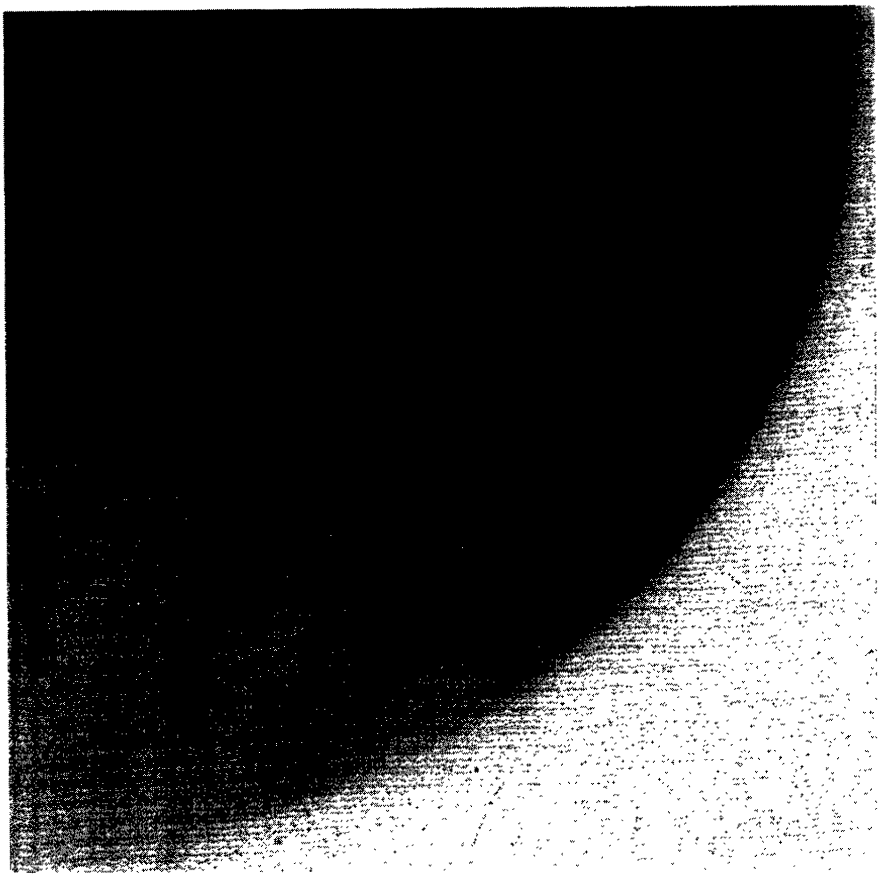

SE quadrant of F plate (MPF 1411) in Lynx.3

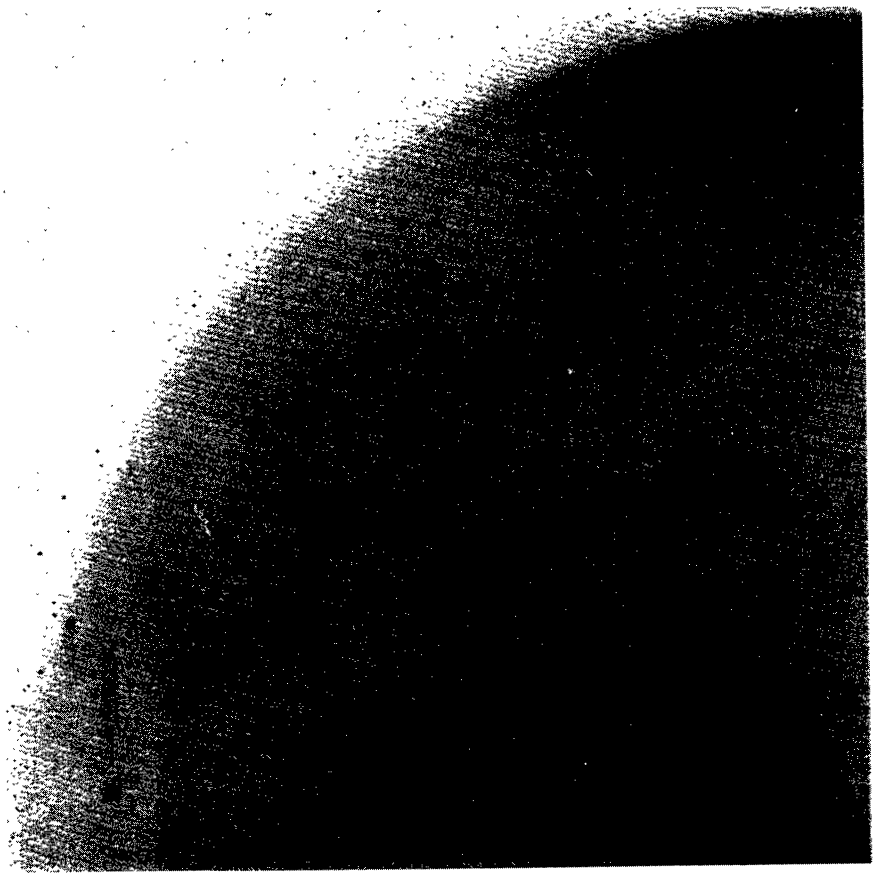

NW quadrant of F plate (MPF 1412) in Lynx.4

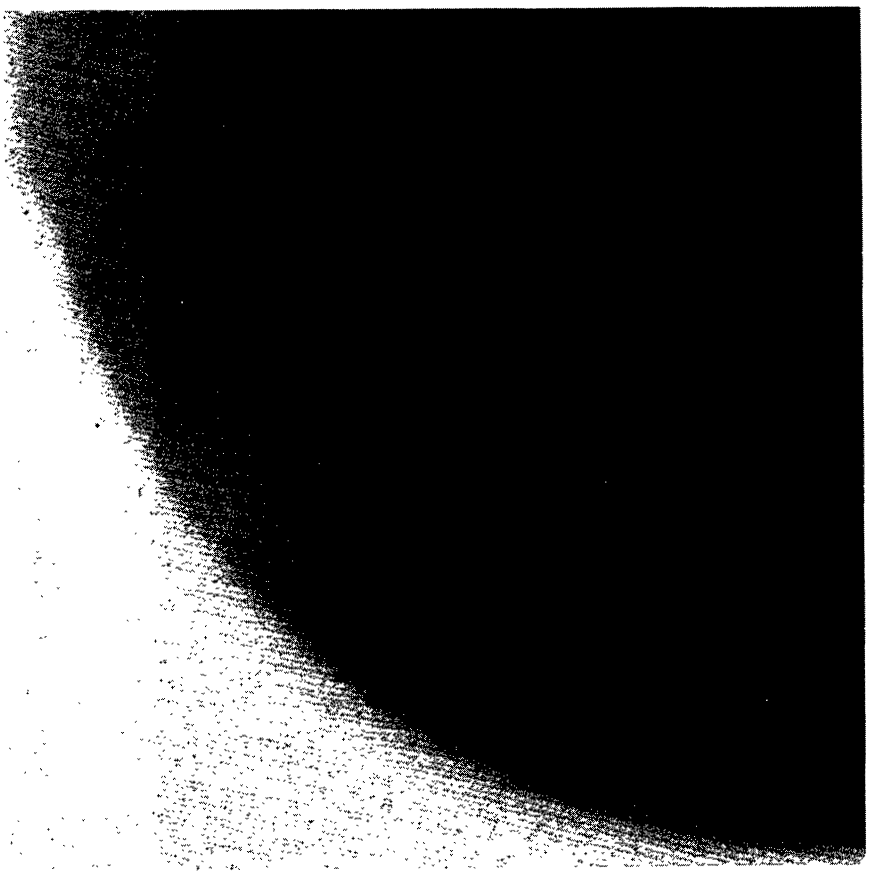

NE quadrant of F plate (MPF 1412) in Lynx.4

SW quadrant of F plate (MPF 1412) in Lynx.4

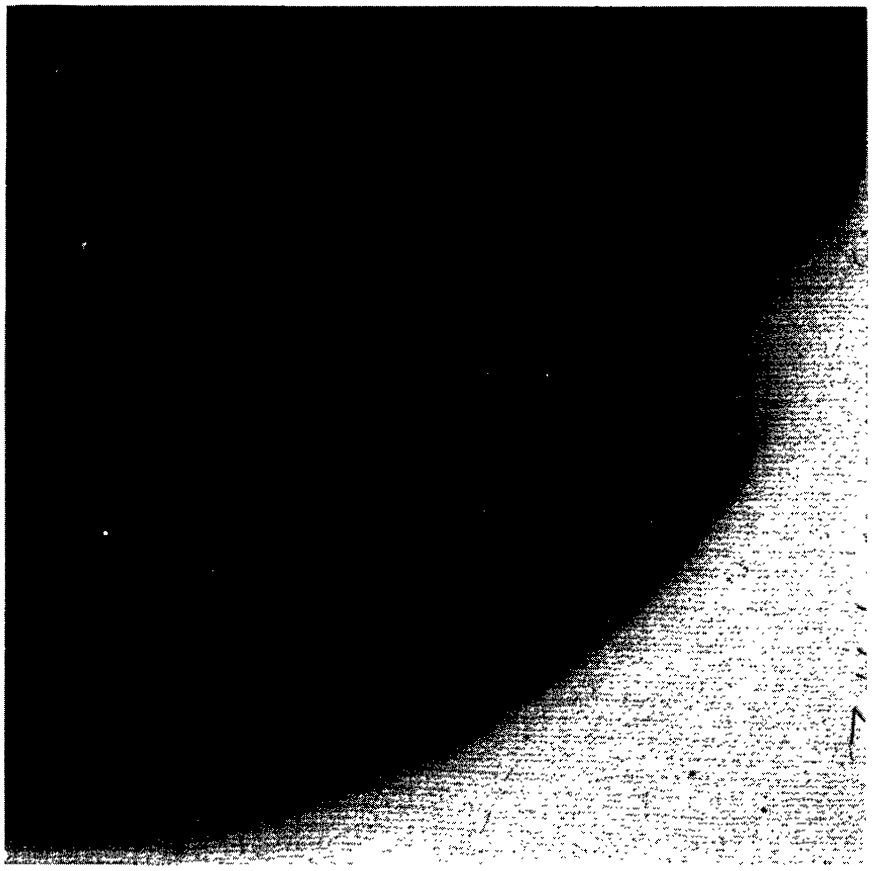

SE quadrant of F plate (MPF 1412) in Lynx.4

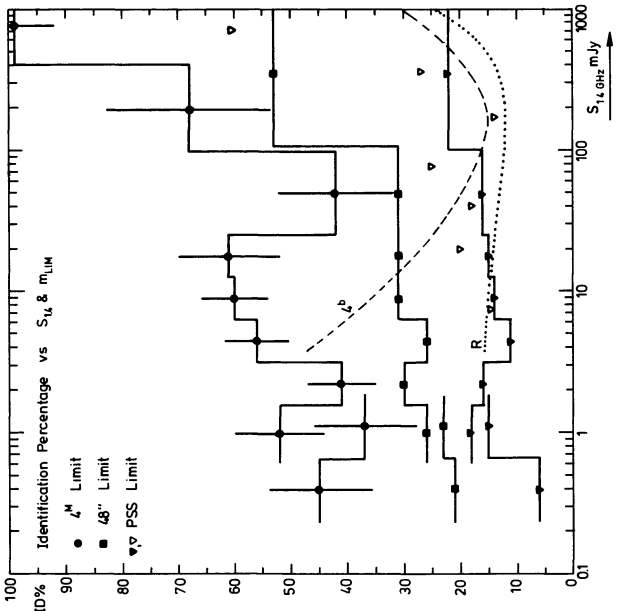

FIGURE 5. — Identification fraction *versus* 1.4 GHz flux and limiting magnitude. Open triangles are data of de Ruiter, Willis and Arp (1979). Model predictions for the PSS limit are shown for model 4b of Wall *et al.* (1980) and the free form model of Robertson (1980).

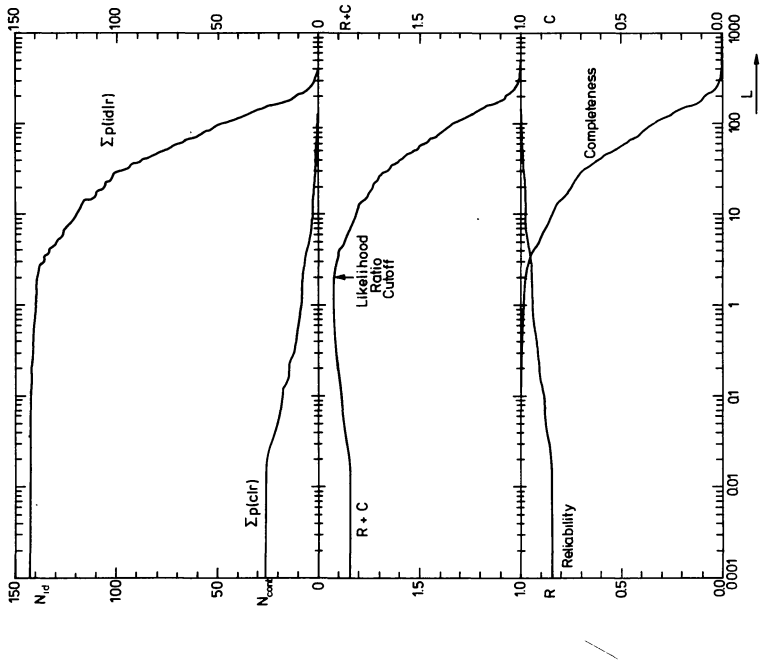

FIGURE 4. — The lower panel is the sample reliability and completeness *versus* likelihood ratio cut-off value L for the 146 candidates with $L > 2.0$. The middle planel is the sum of the two, which peaks at a likelihood ratio cut-off $L \simeq 2.0$. The upper panel gives the expected number of real identifications with $LR \geqslant L$ and the expected number of spurious objects with $LR \geqslant L$.

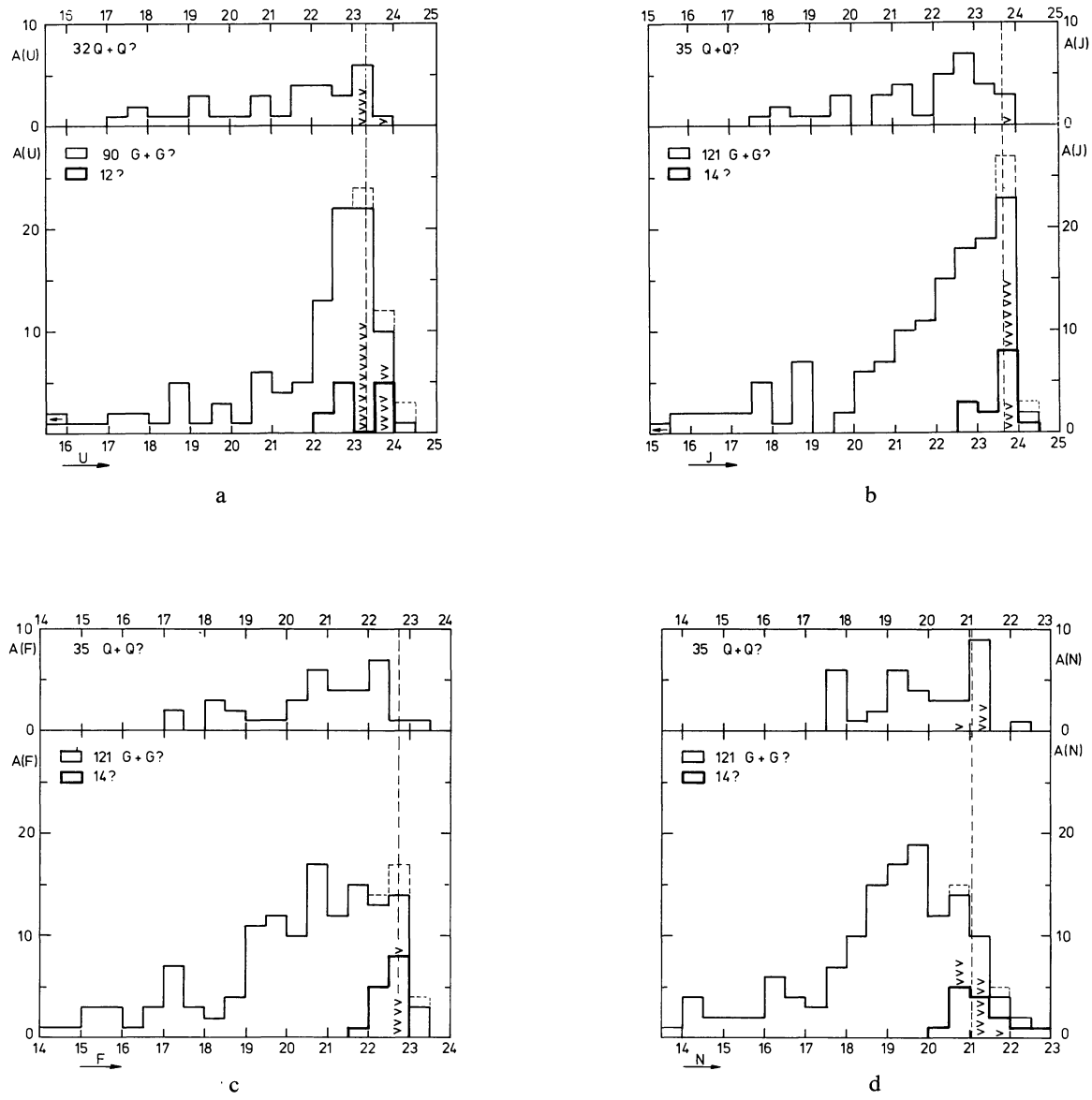

FIGURES 6a-d. — The *U*, *J*, *F*, and *N* magnitude distributions for the complete sample. Objects belong to a complete sample if they are brighter than the plate limits in at least two passbands, the average of which is plotted as a vertical dashed line. If such objects are not visible in one or two other passbands, an upper limit for the corresponding passband is plotted by a « > ». Dashed lines show that only a few more objects are seen if the complete sample is defined as all objects that could be photometered in at least *one* passband. Most upper limits are in *U* and *J*, because some very red galaxies only show up in *F* and *N*.

Following pages.

FIGURE 7. — Multiband images of all identified radio sources, in order of Westerbork number. These photographs are made from a Grinnell display, after scanning the multicolor plates with a PDS microdensitometer, according to the procedure described in Paper III. For all details on the photometry we refer to Paper III. For each object the *U* image is in the lower left, *J* in lower right, *F* in upper left and *N* in the upper right quadrant. The area around each image is 30 arcsec on a side, except that the *U* and *F* images are cut off slightly at the left side. North is up, East is to the left. For each source the identification is centred, except for 55W152 where the identification turned out to be the bright galaxy. *U* data are lacking for Lynx.1 and Lynx.4 (the images appearing in the lower left of Lynx.4 objects are the *J* images repeated). A defect exists on the *N* frame of 53W052. Satellite trails cross some *F* images of SA68. 54W008 was so bright that the sky-normalization failed for the *J* picture. Attention should be given to the occasional intrusion of a secondary image produced by a pickering prism (e.g. the *N* picture of 55W074). The very limited dynamic range of these pictures must be kept in mind when evaluating galaxy morphology.